

1 **Evaluating Cropland N₂O Emissions and Fertilizer**
2 **Plant Greenhouse Gas Emissions with Airborne**
3 **Observations**

4 **A. Gvakharia¹, E. A. Kort¹, M. L. Smith², S. Conley²**

5 ¹Climate and Space Science and Engineering, University of Michigan, Ann Arbor, MI

6 ²Scientific Aviation Inc., Boulder, CO

7 **Key Points:**

- 8 • Reported N₂O and CO₂ emissions from fertilizer plants agree with observations
9 but CH₄ is underestimated by orders of magnitude
10 • We demonstrate mass balance quantification of N₂O emissions from agriculture
11 at 10–100 km scales
12 • Airborne measurements can observe and quantify N₂O emission differences be-
13 tween agricultural fields of ~2.5 km²

This is the author manuscript accepted for publication and has undergone full peer review but has not been through the copyediting, typesetting, pagination and proofreading process, which may lead to differences between this version and the [Version of Record](#). Please cite this article as doi: [10.1029/2020JD032815](https://doi.org/10.1029/2020JD032815)

Corresponding author: Alexander Gvakharia, agvak@umich.edu

Abstract

Agricultural activity is a significant source of greenhouse gas emissions. The fertilizer production process emits N_2O , CO_2 , and CH_4 , and fertilized croplands emit N_2O . We present continuous airborne observations of these trace gases in the Lower Mississippi River Basin to quantify emissions from both fertilizer plants and croplands during the early growing season. Observed hourly emission rates from two fertilizer plants are compared with reported inventory values, showing agreement for N_2O and CO_2 emissions but large underestimation in reported CH_4 emissions by up to a factor of 100. These CH_4 emissions are consistent with loss rates of 0.6–1.2%. We quantify regional emissions fluxes (100 km) of N_2O using the airborne mass balance technique, a first application for N_2O , and explore linkages to controlling processes. Finally, we demonstrate the ability to use airborne measurements to distinguish N_2O emission differences between neighboring fields, determining we can distinguish different emission behaviors of regions on the order of 2.5 km^2 with emissions differences of approximately $0.026 \mu\text{mol m}^{-2} \text{ s}^{-1}$. This suggests airborne approaches such as outlined here could be used to evaluate the impact of different agricultural practices at critical field-size spatial scales.

1 Introduction

Nitrous oxide (N_2O) is the third most important long-lived anthropogenic greenhouse gas (Myhre et al., 2013). It is also currently the most significant anthropogenically emitted gas that depletes stratospheric ozone (Ravishankara et al., 2009). An estimated $16 \text{ Tg N}_2\text{O-N yr}^{-1}$ was emitted globally in the 1990s, with about half coming from anthropogenic sources including agricultural land management, sewage, and biomass burning (Reay et al., 2012). The estimated magnitude of agricultural emissions ranges from $4\text{--}7 \text{ Tg N yr}^{-1}$ and is predicted to rise in the next decade as developing nations increase agricultural productivity (FAO, 2017). The large uncertainty in emissions estimates is a result of both infrequent measurements with limited coverage being insufficient to characterize emissions that exhibit high spatial and temporal variability (Monni et al., 2007) and the lack of direct measurements to get accurate emission factors from all sources (Brown et al., 2001).

A dominant source of anthropogenic N_2O has been the mass production and application of fertilizer. Since 1908 the Haber-Bosch process of synthesizing ammonia and producing nitric acid, ammonium nitrate, and other compounds has allowed for mass pro-

46 production of synthetic fertilizer, with current global production levels near 100 Tg N yr⁻¹
47 (Erisman et al., 2008; Smil, 2011). Between 1961–2013 global N fertilizer consumption
48 increased by a factor of nearly 10, with 5 countries accounting for over 60% of the con-
49 sumption (Lu & Tian, 2017). In the United States the current fertilizer application rate
50 is 11.4 Tg N yr⁻¹, a ~40 times increase since 1940 (Cao et al., 2018). Fertilizers pro-
51 vide essential nutrients to plants that enhance their growth and yield but soils have a
52 limited nutrient uptake capacity, and over-application of nitrogen fertilizer can cause a
53 nonlinear increase in N₂O emissions (Grant et al., 2006).

54 Fertilizer production itself also emits greenhouse gases and differences in produc-
55 tion type and efficiency affect the total footprint of synthetic fertilizer (Fossum, 2014).
56 Ammonia production is energy-intensive, requiring the combustion of natural gas or other
57 fuels to synthesize nitrogen and hydrogen (Gellings & Parmenter, 2016). Facilities may
58 then oxidize ammonia to produce nitric acid, which is used to manufacture ammonium
59 nitrate fertilizer (EFMA, 2000). Ammonia oxidation emits waste gases, including N₂O
60 (EFMA, 2000). In 2017 fertilizer plants accounting for 73% of total US nitrogen produc-
61 tion capacity emitted 23 Tg of CO₂ equivalent (CO₂e) greenhouse gas emissions (TFI,
62 2017). N₂O and CH₄ emissions are converted to CO₂e values by multiplying by global
63 warming potential values of 298 and 25, respectively. Though facilities report emissions,
64 independent objective observations of production sources have been limited.

65 While fertilizer is arguably the strongest driver of N₂O soil emissions, various fac-
66 tors including climate, soil conditions, planted crop type, and management practices can
67 impact N₂O emissions, leading to large spatial and temporal heterogeneity in emissions.
68 Increased N₂O emissions can positively correlate with higher soil temperature and mois-
69 ture, particularly after precipitation (Dobbie et al., 1999; Griffis et al., 2017). The pos-
70 itive relationship between N₂O emissions and soil moisture has been observed in vari-
71 ous environments and soil conditions (K. A. Smith et al., 1998, 2003; Marinho et al., 2004;
72 Schindlbacher et al., 2004; Pattey et al., 2008). Crop species and type of residue crop
73 cover can also affect emissions (T. B. Parkin & Kaspar, 2006; Lemke et al., 2018).

74 Flux chambers are a commonly-used method to quantify N₂O emissions from soils.
75 They are relatively inexpensive and easy to deploy, but measure small areas (1 m²), can
76 perturb the area of study, and are constrained by manpower (Rapson & Dacres, 2014).
77 Scaling up singular chamber measurements for greater representation of emissions is ham-

78 pered by soil diversity and spatial variability (T. Parkin et al., 2012; Scaroni et al., 2014),
79 necessitating data at larger regional spatial resolution. Studies at larger scales can also
80 capture indirect emissions from nitrogen runoff and leaching. Process-based models work
81 at a range of scales (Del Grosso et al., 2006; Tian et al., 2012) but have uncertainty in
82 their representation, demand high computational power and often have large input un-
83 certainties. This increases the need to use observational data at a range of scales to re-
84 duce uncertainty (Butterbach-Bahl et al., 2013; Ehrhardt et al., 2017). Improved obser-
85 vational quantification of emissions on varying spatial scales will be critical to improve
86 our understanding of the heterogeneous processes controlling N₂O emissions.

87 Many studies of US N₂O emissions have investigated the Corn Belt region of the
88 Upper Mississippi River Basin (T. B. Parkin & Kaspar, 2006; Chen et al., 2016; Nevi-
89 son et al., 2018). Relatively less attention has been paid to the Lower Mississippi River
90 Basin (LMRB) downstream in the southeast US, which was only recently added in 2014
91 to the USDA's Long-Term Agroecosystem Research (LTAR) network (USDA ARS, 2014).
92 With ~20 million acres—~30% of total area—as cropland, much of it intensely devel-
93 oped and irrigated, the LMRB is a highly-productive agricultural region responsible for
94 a quarter of the US's corn production and two-thirds of its rice (USDA ARS, 2012; Lund
95 et al., 2013).

96 Here we analyze continuous airborne observations of N₂O, CO₂, and CH₄ from re-
97 search flights in the LMRB in May 2017 during the early growing season (Padgitt et al.,
98 2000; Snipes et al., 2004). The campaign took place immediately following a heavy rain-
99 fall and flooding event in the northern part of the region (Heimann et al., 2018). We quan-
100 tify emissions of N₂O, CO₂, and CH₄ from two large fertilizer plant point sources and
101 compare to reported emissions from the Greenhouse Gas Reporting Program (GHGRP).
102 We apply the airborne mass balance technique to N₂O to quantify emission fluxes on scales
103 on the order of 100 km², and evaluate relationship with crop type, applied fertilizer, soil
104 moisture, and soil temperature. We further use a Bayesian inversion method to deter-
105 mine the potential of this type of airborne data to distinguish emission differences from
106 neighboring agricultural fields.

2 Methods

2.1 Flights

Research flights were conducted on a Mooney M20R single-engine aircraft (Scientific Aviation, Inc.) as part of the Fertilizer Emissions Airborne Study (FEAST) (Gvakharia et al., 2018; E. Kort et al., 2018). Six research flights took place from May 2–10, 2017, based out of West Memphis, Arkansas. Each flight typically lasted ~6 hours from 12:00–18:00 local time (17:00–23:00 UTC), sampling once a well-mixed boundary layer developed. Combined, the flights covered most of the LMRB region, from 31° to 38°N and 88° to 93°W. The plane flew at an average altitude of 550 meters above ground level (magl), with multiple crosswind transects designed to capture emissions plumes from agricultural activity in the river valley. During each flight at least one vertical profile was completed, circling the plane up past the mixing layer and back down while tracking atmospheric conditions and trace gases to determine the mixed layer depth. On two flights, two high-production fertilizer plants were circled to quantify point source emissions. Figure 1 shows the region of study with flight paths, along with land use for four major crops: soybean, corn, cotton, and rice.

2.2 Instrumentation

An Aerodyne laser absorption spectrometer measured N₂O, CO₂, CO, and H₂O mole fractions at 1 Hz frequency with an in-flight high-frequency, flow-controlled calibration method (Frequent Calibration High-performance Airborne Observation System (FCHAOS)) as described in Gvakharia et al. (2018). In-flight 1 s precisions were ±0.05 ppb, ±0.10 ppm, ±1.00 ppb, and ±10 ppm respectively for N₂O, CO₂, CO, and H₂O. Water vapor corrections were applied to the data in post-processing to eliminate the effect of dilution and water line broadening—all measurements reported herein are dry molar fractions.

Additional payload on the aircraft, listed in S. A. Conley et al. (2014); S. Conley et al. (2017), included a Picarro G2301-f cavity ringdown spectrometer to measure CH₄, CO₂, and H₂O (with in-flight precision of ±0.3 ppb and ±0.04 ppm for CH₄ and CO₂, respectively (Karion et al., 2013)), a Vaisala HMP60 probe to measure temperature and relative humidity, and a 2B Technologies 202 ozone monitor. The Picarro measurements were sampled at 0.5 Hz and interpolated to acquire 1 Hz data. The Picarro was calibrated

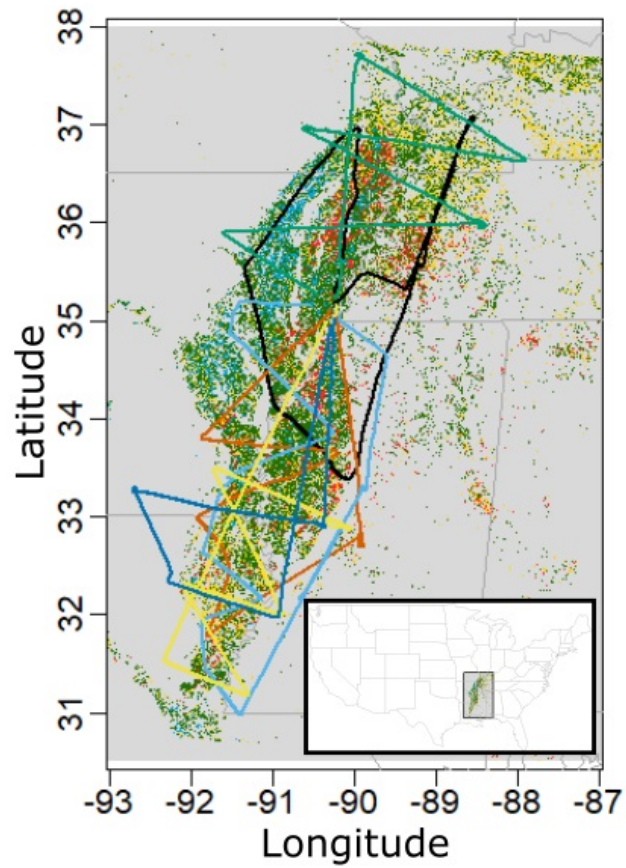


Figure 1. Map of the LMRB. FEAST research flights paths are traced with different colors for each flight. Green, yellow, red, and blue pixels respectively indicate cropland for soybean, corn, cotton, and rice at 30 m by 30 m resolution (USDA, 2017).

138 on the ground by sequentially sampling two gravimetrically-prepared NOAA WMO stan-
 139 dards (Dlugokencky et al., 2005). Wind speed and direction were calculated using a dif-
 140 ferential GPS system as described in S. A. Conley et al. (2014). Ambient air was sam-
 141 pled from an inlet installed underneath the aircraft wing, and traveled through ~ 5 m
 142 of tubing to the instruments. Lag time between when air enters the inlet line and when
 143 it is sampled by the instruments was determined by breathing near the inlet and observ-
 144 ing spikes in CO_2 and H_2O , resulting in lag times of 3 and 5 s for the Aerodyne and Pi-
 145 carro instruments respectively. These lag times were confirmed in flight by comparing
 146 peaks in CO_2 and H_2O from both instruments. The lag times are used in post-processing
 147 to align all instruments and sensors on a unified time basis.

148 2.3 Point Source Quantification

149 Emission rates from point sources are quantified following the methodology first
 150 described in S. Conley et al. (2017) and used by Mehrotra et al. (2017); Vaughn et al.
 151 (2017). Figure 2 illustrates the technique. The plane circles a source at constant radius
 152 and at discrete altitudes, starting near 200 magl and ascending until the plume is no longer
 153 detectable, then descending back down. By measuring the atmospheric concentration
 154 upwind and downwind of the source simultaneously with the wind, an emission rate is
 155 calculated for a given trace gas. As described in S. Conley et al. (2017), the method in-
 156 tegrates sources and sinks of a gas species within a cylindrical volume V around an emis-
 157 sion source. Using Gauss’s theorem the volume integral can be converted into a surface
 158 integral decomposing the cylinder into three surfaces: bounded vertically at the bottom
 159 by the ground and at the top by the altitude where the plume is no longer detected (z_{max}),
 160 and horizontally by the radius of the flight loops. The basis for the methodology is given
 161 by Equation 1

$$Q_c = \left\langle \frac{\partial m}{\partial t} \right\rangle + \int_0^{z_{max}} \oint c' u_h \cdot \hat{n} dl dz \quad (1)$$

162 where $\left\langle \frac{\partial m}{\partial t} \right\rangle$ is the average rate of change of mass in the volume, c' is the devia-
 163 tion of the gas species of interest from the loop average, u_h is the horizontal wind vec-
 164 tors, and \hat{n} is an outward pointing unit vector normal to the surface. Large-eddy sim-
 165 ulations results from S. Conley et al. (2017) show that the flux divergence changes quick-
 166 est closer to the source, making it more difficult to measure, while further away from the

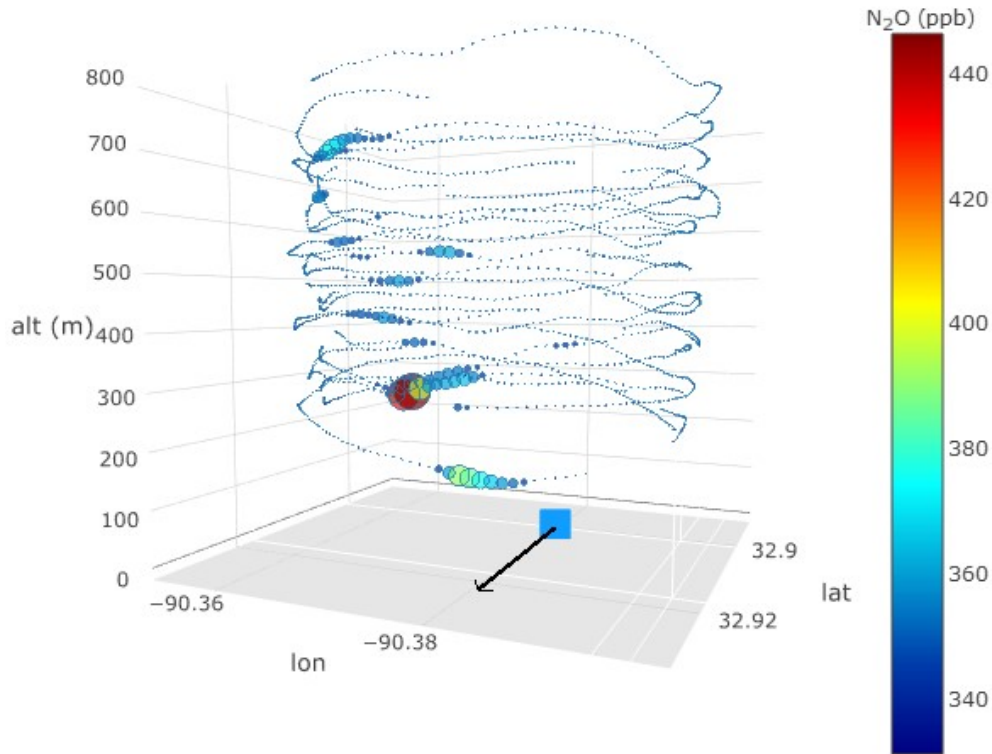


Figure 2. Flight pattern during point source quantification. The blue square shows the location of the emitting source, in this case a fertilizer plant, and the black arrow indicates wind direction. N_2O molar fraction is given both by the color bar and the point size. The plane circles the source upwind and downwind at several altitudes, capturing the emissions plume, and the data is then processed to quantify an emissions flux.

167 source the plume is weaker and susceptible to entrainment fluxes. An appropriate sam-
 168 pling radius is determined in-flight based on the boundary layer height and horizontal
 169 wind speeds to ensure that the plane is far enough so the plume has time to loft verti-
 170 cally, minimizing change in flux divergence, but not too far that the plume signal is dif-
 171 ficult to detect against background. The loops are then divided into bins, with the low-
 172 est bin extending to the ground. Individual bin uncertainty is given by the standard de-
 173 viation of horizontal flux uncertainty, which is higher at lower altitudes where the flux
 174 divergence has a higher rate of change. The total uncertainty is then obtained by sum-
 175 ming all bin uncertainties in quadrature (along with uncertainty from the time rate of
 176 change term from Equation 1, which is determined using a least squares fit on the gas
 177 density with time and altitude).

Table 1. CO₂ emission rates based on both FCHAOS and Picarro observations from two fertilizer facilities

Plant	FCHAOS CO ₂ (Mg hr ⁻¹)	Picarro CO ₂ (Mg hr ⁻¹)
Plant 1	98.3±24	94.6±21.4
Plant 1	94.4±17.6	109.1±24.7
Plant 2	73.6±15.7	88.1±19.3

178 Due to the FCHAOS system's frequent calibrations to on-board gas standards, 15
 179 s of data were not sampled every 120 s. When quantifying N₂O and CO₂ emission rates,
 180 the FCHAOS data are interpolated to fill in gaps throughout the loops. As seen in Ta-
 181 ble 1, CO₂ estimates agree between the FCHAOS and the Picarro (which has no data
 182 gaps), suggesting this interpolation does not significantly impact this analysis.

183 2.4 Mass Balance Technique

184 Using the mass balance method (White et al., 1976), atmospheric N₂O fluxes are
 185 quantified for regions in the LMRB. The usefulness of this approach has been well-documented
 186 in estimates of methane (Karion et al., 2015; Peischl et al., 2015; M. L. Smith et al., 2017),
 187 ethane (M. L. Smith et al., 2015; E. A. Kort et al., 2016), and black carbon (Schwarz
 188 et al., 2015) emissions from oil and natural gas activity. The flux during a flight tran-
 189 sect is given by Equation 2

$$flux_{N_2O} = \nu \cos\theta \int_{x_i}^{x_f} X_{N_2O} dx \int_{z_g}^{z_1} n_{air} dz. \quad (2)$$

190 where $\nu \cos\theta$ is the horizontal wind component perpendicular to the airplane's heading,
 191 x_i and x_f define the width of the flight transect over ground, X_{N_2O} is the N₂O molar
 192 fraction enhancement over background during the transect, and z_g is the terrain height
 193 above sea level. z_1 is the adjusted mixed layer height as defined in Peischl et al. (2015),
 194 $z_1 = (3z_{PBL} + z_e)/4$ where z_{PBL} is the planetary boundary layer depth and z_e is the
 195 entrainment height at which mixing below the boundary layer finally reaches free tro-
 196 posphere levels (always $\geq z_{PBL}$). n_{air} is the molar density of air. Background N₂O is
 197 determined by averaging 30 s of data at the start and end of a plume, i.e. the times defin-
 198 ing the width of the transect with enhancement over background. Uncertainty for mix-
 199 ing layer height is defined as $\Delta z = z_1 - z_{PBL}$, while for the other components it is defined

200 by the 1σ value. All uncertainties are then propagated by summing in quadrature for
 201 the total flux uncertainty, assuming independent and normally-distributed errors.

202 For each flight mass balance transects are identified and an N_2O flux is calculated
 203 using Equation 2. Emissions are then quantified from a subregion bounded by two tran-
 204 sects by subtracting the flux of the upwind transect (or “flux in”) from the flux of the
 205 downwind transect (or “flux out”). Transects are chosen such that a transect with length
 206 l_i and mean angle of wind normal to the aircraft θ_i has a similar $l_i \cos\theta_i$ value as another
 207 transect with $l_j \cos\theta_j$. The air mass passes through two planes with equal areas defined
 208 by $l \cos\theta z_1$, allowing comparison of fluxes from different transects.

209 We compare regional mass balance fluxes with crop type, applied fertilizer, soil mois-
 210 ture, and soil temperature. Crop land cover for 2017 is provided by the Cropland Data
 211 Layer (CDL) at 30 m resolution (USDA, 2017). A 5 km resolution gridded dataset of
 212 annual applied nitrogen fertilizer provides nitrogen input information (Cao et al., 2017).
 213 The data used is from 2015, the most recent year available in the dataset. As of writ-
 214 ing, gridded U.S. fertilizer application data with high spatial resolution for 2017 had not
 215 been identified. Two soil moisture data sets are used in this analysis. The first is the SMAP
 216 Enhanced L3 Radiometer Global Daily 9 km EASE-Grid Soil Moisture, Version 2 data
 217 product from the Soil Moisture Active Passive (SMAP) satellite (O'Neill et al., 2018).
 218 While the satellite provides good spatial resolution, the area it scans on each pass of the
 219 earth does not always coincide with the flight path. In order to estimate regional soil mois-
 220 ture during a flight, the SMAP products from May 1–10, 2017 are averaged over the LMRB
 221 region. The second soil moisture data set is the North American Regional Reanalysis (NARR)
 222 product which combines model output and assimilated precipitation data at 0.3° reso-
 223 lution (Mesinger et al., 2006). To complement volumetric water content, water-filled pore
 224 space (WFPS) is also calculated to better relate soil properties. WFPS is defined by Linn
 225 and Doran (1984) in Equation 3

$$WFPS = \frac{\Theta_v}{1 - \frac{P_B}{P_P}} \quad (3)$$

226 where Θ_v is volumetric water content, P_P is soil particle density, and P_B is soil bulk den-
 227 sity. A common P_P value of 2.65 g cm^{-3} is used (Soane, 1990). For P_B , an average value
 228 of 1.385 g cm^{-3} is used based on measurements of soil density in the LMRB (Römken-
 229 et al., 1986; Selim et al., 1987; Scott et al., 1998). NARR is also used for soil temper-
 230 ature data (Mesinger et al., 2006). The mass balance fluxes are correlated with environ-

231 mental drivers using observed hourly flux values and comparing with environmental data
 232 averaged over the spatial region defined by the mass balance transect.

233 2.5 Bayesian Inversion and STILT

234 To evaluate the spatial scales and flux magnitudes we can associate with small scale
 235 observed airborne variability, we use a simple inversion approach. First we selectively
 236 focus on small-scale features (plumes, ~ 10 s) observed in the aircraft data. By isolating
 237 this portion of our data set we can then use an inversion method to determine areal ex-
 238 tent and flux magnitudes that explain the observed signals. We calculate posterior fluxes
 239 of N_2O in the LMRB using the Bayesian solution to the inverse problem given by Equa-
 240 tion 4 (Rodgers, 2000)

$$\hat{s} = s_0 + (Q^{-1} + H^T R^{-1} H)^{-1} H^T R^{-1} (z - H s_0) \quad (4)$$

241 where \hat{s} is a vectorized gridding of posterior fluxes with length m and units μmol
 242 $\text{m}^{-2} \text{s}^{-1}$, s_0 is the vectorized gridding of prior flux with length m and units μmol
 243 $\text{m}^{-2} \text{s}^{-1}$, z is a vector of N_2O enhancements from flight observations with length n and units
 244 ppm, H is the Jacobian matrix of sensitivity in the transport model with size $n \times m$ and
 245 units $\text{ppm}/(\mu\text{mol} \text{m}^{-2} \text{s}^{-1})$, Q is the prior error covariance matrix with size $m \times m$ and
 246 units $(\mu\text{mol} \text{m}^{-2} \text{s}^{-1})^2$, R is the model-data mismatch covariance matrix with size $n \times$
 247 n and units ppm^2 .

248 We assume model-data mismatch errors are uncorrelated and construct R as a di-
 249 agonal matrix with σ_R^2 as its components, with $\sigma_R = 0.01$ ppb, the 1 s precision for our
 250 N_2O observations. Similarly, for Q we construct a diagonal matrix with σ_Q^2 components,
 251 with the value of $\sigma_Q = 0.01 \mu\text{mol} \text{m}^{-2} \text{s}^{-1}$ based on optimizing predicted enhancements.
 252 We used a flat prior of $0.0001 \mu\text{mol} \text{m}^{-2} \text{s}^{-1}$ based on typical values from flux chamber
 253 studies such as Marinho et al. (2004) and T. B. Parkin and Kaspar (2006). Our input
 254 parameters for the Bayesian inversion are not optimized to provide true absolute esti-
 255 mates of fluxes in the entire region, rather we are interested in quantifying relative fluxes
 256 and spatial extents at a spatial scale between that of the point source quantification and
 257 the regional mass balance. Instead of performing a full campaign inversion to calculate
 258 gridded optimized fluxes, we are evaluating the spatial scales and magnitudes of fluxes
 259 from local enhancements to assess the airborne measurement system's performance and
 260 ability to resolve individual field-scale emissions.

We construct the Jacobian H using footprints obtained from running the Stochastic Time-Inverted Lagrangian Transport (STILT) model (Gerbig et al., 2003; Lin et al., 2003) using the High-Resolution Rapid Refresh (HRRR) meteorology data (Benjamin et al., 2016). We run STILT for 102 receptors from the May 2 research flight, sending 333 particles back in time for 4 hours (sufficient for the trajectories to clear the LMRB cropland) for each receptor at 1 minute resolution. All the receptors come from two eastern transects in the flight that experienced a large regional N_2O enhancement. The receptors were chosen by identifying local N_2O features (coherent enhancements, or plumes), and were organized into 13 distinct enhancements for individual evaluation to determine what upwind area and emissions produced these observed signals. The lowest observed N_2O concentration in each group was used as a local background value and subtracted from the group to obtain enhancements used in the z vectors in Equation 4. Footprints were calculated from the particle trajectories as in Lin et al. (2003) with a 0.005° resolution in latitude and longitude, or about 500 m.

3 Results

3.1 Fertilizer Plant Emissions

Two large fertilizer plants with significant greenhouse gas emissions are investigated. These are 2 of 19 facilities in the US with reported N_2O emissions greater than 100 Gg CO_2e (EPA, 2017). Plant 1 was responsible for 5% of all US emissions of N_2O in 2017, and Plant 2 contributed 1% (EPA, 2017). In terms of ammonia production, 32 plants in the US accounted for 10500 Gg N (USGS, 2018). Plant 1's ammonia production capacity is equal to 4% of the total US ammonia production, while Plant 2's capacity is 3.5% (Nutrien, 2018). Figure 3 shows N_2O and CO_2 quantified emission rates from the FCHAOS system, CO_2 and CH_4 emission rates from the Picarro, and reported GHGRP emissions for both plants. The GHGRP emissions are scaled down from Tg yr^{-1} to kg hr^{-1} accounting for 340 days of effective production capability (USGS, 2019), as fertilizer production facilities typically operate non-stop throughout the year with some periodic maintenance, resulting in low temporal variability (TFI, 2017). Plant 1 was observed on both May 9 and May 10, while Plant 2 was observed only on May 10. Estimates for N_2O and CO_2 agree well within uncertainty with emissions reported in the GHGRP. For Plant 1, there is also consistency in emissions from one day to the next.

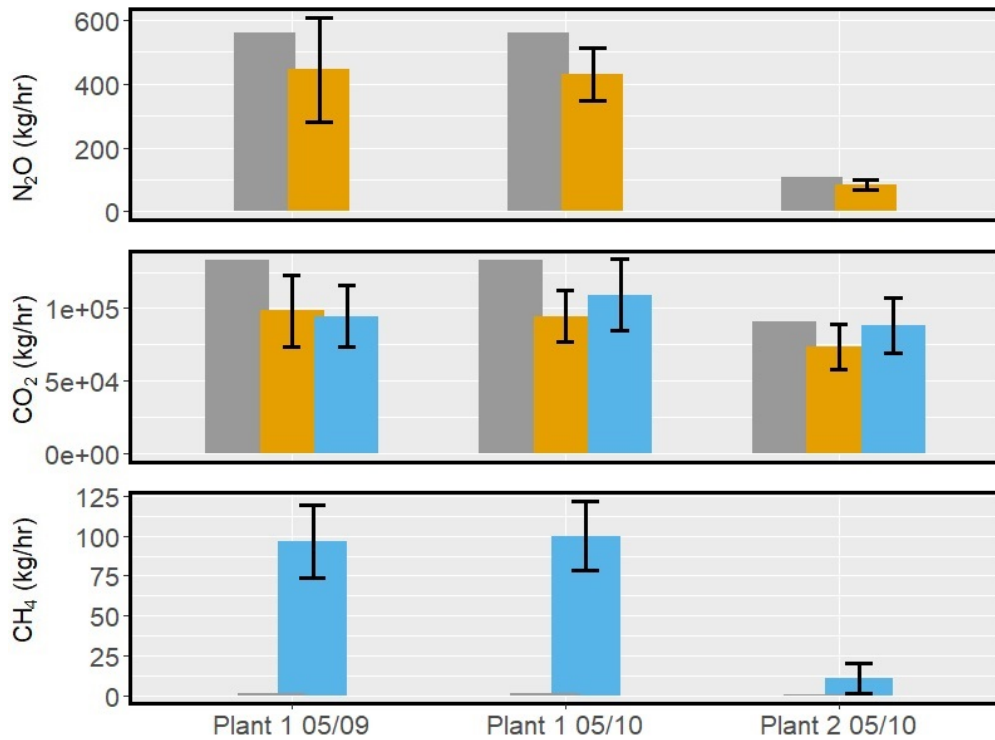


Figure 3. Observed emissions for N_2O , CO_2 , and CH_4 (FHCAOS in orange, Picarro in blue) along with 2017 GHGRP data (gray) for two fertilizer plants from EPA (2017). Black error bars indicate 1σ uncertainty.

292 CH₄ estimates are underestimated in the reported values compared to our obser-
293 vations, by a factor of 100 for Plant 1 and 20 for Plant 2. According to the GHGRP, 100%
294 of the CH₄ emissions from both plants is a result of stationary fuel combustion (EPA,
295 2017). Using the amount of gas combusted, a leakage rate is calculated to account for
296 the discrepancy in observed and reported emissions. Plant 1 directly reports the amount
297 of natural gas consumed while Plant 2 does not, but the value is calculated using reported
298 emissions and GHGRP-defined emission factors. Using a typical natural gas composi-
299 tion range of 70–90% CH₄ (Speight, 2007) results in a range in leakage rates of 0.6–0.8%
300 for Plant 1 and 0.9–1.2% for Plant 2. However, CH₄ accounts for ~0.01% of total GHGRP-
301 reported CO₂e emissions for both plants, with N₂O and CO₂ contributing essentially all
302 of the GHG emissions. Adding in observed CH₄ emissions changes the contribution of
303 methane to 0.9% for Plant 1, a factor of 90 increase, and 1.8% for Plant 2, a factor of
304 180 increase. This finding is in agreement with observations of CH₄ from six different
305 fertilizer plants by Zhou et al. (2019). Their study found CH₄ to be underestimated rel-
306 ative to the GHGRP by factors of 50–175 for five of the plants and by 3250 for the sixth,
307 resulting in a worst-case leakage rates of 1.22% and a nominal-case rate of 0.34%.

308 3.2 Regional N₂O Fluxes

309 N₂O fluxes are calculated from mass balance transects for 26 regions, ranging from
310 the northern end of the LMRB near the Missouri/Kentucky border down to the south-
311 ern end of the valley in northern Louisiana. Figure 4 illustrates an example flight path
312 and N₂O enhancement from May 9. The typical background approach is to use the edges
313 of the enhancement, as shown in Figure 4. For some enhancements the aircraft did not
314 fully exit the area of enhancement in the valley. In these situations, background values
315 from upwind transects are used to account for passive enhancement captured in the down-
316 wind transect.

317 For all regions, the mean emission flux is 1.0 ± 0.7 g N₂O-N ha⁻¹ hr⁻¹. Marinho
318 et al. (2004) observed emissions from Mississippi Alluvial Plain soils of 1.5 g N₂O-N ha⁻¹
319 hr⁻¹ following rainfall in mid-June during the growing season, while Scaroni et al. (2014)
320 reported emissions of 0.1 g N₂O-N ha⁻¹ hr⁻¹ from soils in the Louisiana river basin in
321 June and July. From a flux chamber study in Iowa, T. B. Parkin and Kaspar (2006) re-
322 ported soybean crop emissions of ~2500 g N₂O-N ha⁻¹ yr⁻¹, with typical hourly fluxes
323 on the order of 1.5–2.4 g N₂O-N ha⁻¹ hr⁻¹ from soybean, consistent with the results of

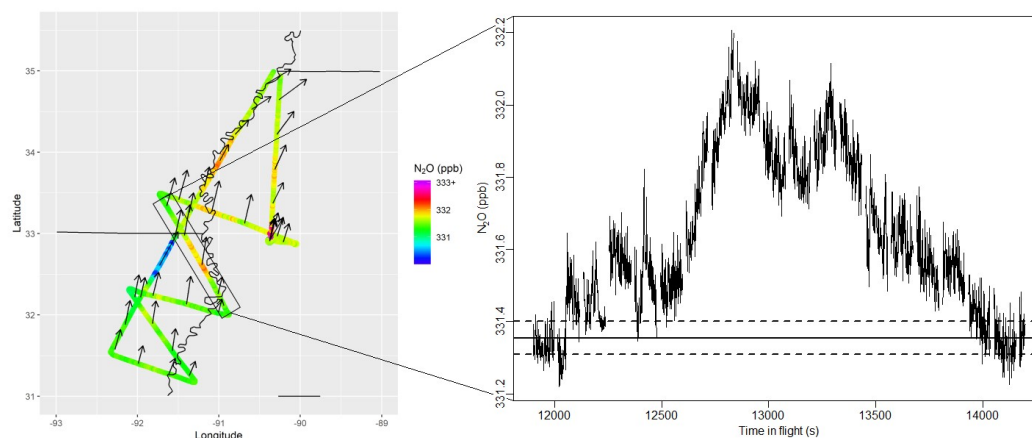


Figure 4. a) Flight path for May 9, 2017, colored by N_2O mole fraction. Black arrows indicate wind direction and relative magnitude. The black box highlights a transect used for mass balance. b) The N_2O mole fraction along the transect indicated by the black box in a). The first and last 30 s of the transect are used to find the mean background and its 1σ uncertainty (solid black line and dashed lines, respectively).

324 this analysis. T. B. Parkin and Kaspar (2006) report fertilizer application in Iowa oc-
 325 ccurring on day 155 of the year, while the FEAST campaign took place from day 122 to
 326 130. However, crop planting in the LMRB typically occurs earlier than the Corn Belt
 327 according to the USDA's Crop Progress Reports (USDA NASS, 2017b). By May 7, 2017,
 328 based on fraction of state crop acreage for a particular crop, Arkansas, Kentucky, Louisiana,
 329 Mississippi, Missouri, and Tennessee had planted 50–76% of soybean, 50–77% of corn,
 330 7–68% of cotton, and 67–92% of rice (USDA NASS, 2017b, 2017a).

331 The regional mass balance fluxes are compared with crop type, applied fertilizer,
 332 soil moisture, and soil temperature. When we consider environmental drivers individ-
 333 ually, we do not find strong empirical linkages to emissions at this scale. For crop type
 334 and fertilizer application, there is no evident relationship. A weak linear dependence is
 335 observed for soil moisture ($R^2 = 0.19$) from SMAP, in line with literature (K. A. Smith
 336 et al., 1998; Dobbie et al., 1999; Schindlbacher et al., 2004), and a WFPS relationship
 337 similar to that observed by K. A. Smith et al. (1998), but not for NARR data. With soil
 338 temperature, we observed a temporal gradient, with higher temperatures during later
 339 flights, but temperature alone does not appear to be a strong predictor of N_2O flux com-
 340 pared with exponential relationships in literature (K. A. Smith et al., 1998). The WFPS

341 analysis would potentially be improved using a gridded soil product to provide more re-
342 fined values of P_P and P_B .

343 To assess the relative emergent role of these driving variables, we perform a mul-
344 tiple linear regression analysis with crop type, applied fertilizer, soil moisture, and soil
345 temperature to predict N_2O flux. The resultant fit has $R^2 = 0.64$, $p = 0.01$. By consid-
346 ering multiple environmental driver simultaneously, we find significant empirical relation-
347 ships between drivers and emissions. The strongest predictors that emerge from this anal-
348 ysis are soil moisture from SMAP, and total planted area of soybean, cotton, and rice.
349 A multiple linear regression model with only those four variables has $R^2 = 0.54$, $p = 0.001$.
350 Although fertilizer is expected to be a strong driver of N_2O emissions, the temporal el-
351 ements of its application are not represented by annual data. Since this analysis relates
352 hourly N_2O emissions to annual fertilizer application, it is understandable that the fer-
353 tilizer does not significantly predict N_2O . The crop type may be acting as a proxy for
354 the actual applied fertilizer amount, capturing fertilizer timing and variation in manage-
355 ment practice. While previous studies have observed a positive relationship between emis-
356 sions and soil temperature, it is possible that the soil temperature effect is being dwarfed
357 by other factors such as soil moisture.

358 3.3 Discriminating Field-scale emission differences

359 Whereas the mass balance approach enables robust quantification of large regional
360 areas, a different approach is warranted to evaluate if specific agricultural fields (or clus-
361 ters of fields) exhibit different emissions. We consider a feature in the airborne measure-
362 ments such as illustrated in Figure 5. Using the STILT inversion approach described ear-
363 lier, we then derive optimized emission fields that produce the observed N_2O enhance-
364 ment in this small time window.

365 To evaluate what area most contributed to the observed peak, we consider a 50%
366 threshold value, identifying the highest-enhancement grid cells which contributes 50%
367 of the predicted enhancement. These are the most intense local sources responsible for
368 the observed N_2O concentration. We then use the boundaries defined by these grid cells
369 to quantify the magnitude of fluxes and the areas which contribute the most to the en-
370 hancement - determining the area responsible for the observed feature. Finally, we can
371 compare the average flux of the peak enhancement to the fluxes of the shoulders, defin-

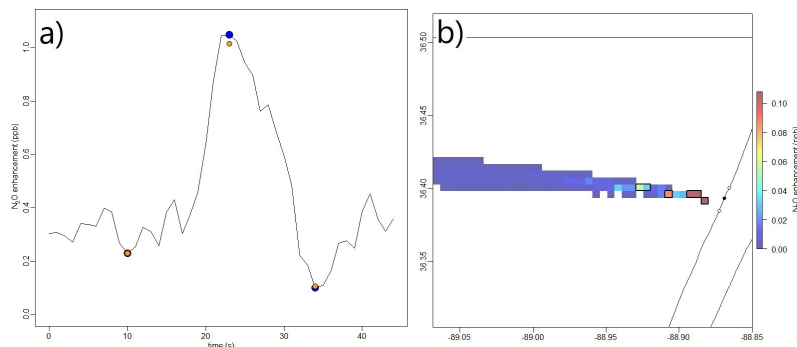


Figure 5. a) Observed (blue points) and predicted (orange points) N₂O enhancements for a group of three receptors in a feature. b) Predicted enhancement grid for the peak enhancement (middle receptor from a)), with a contour around the grid cells that contribute 50% of the total enhancement.

372 ing the relative flux responsible for the observed local feature. Figure 5 illustrates the
 373 observed and predicted enhancements for one group of receptors. We perform this ex-
 374 ercise for 13 different cases.

375 We find an average relative flux of $0.026 \pm 0.01 \mu\text{mol m}^{-2} \text{s}^{-1}$ in the 50% thresh-
 376 old grid cells when comparing the peak enhancement from each group to the local back-
 377 ground. The average observed peak enhancement linked to these fluxes is 0.79 ± 0.26 ppb
 378 N₂O. Our airborne instrument precision is 0.05 ppb with traceability to standards of 0.28
 379 ppb. In conditions experienced in these flights, we thus can robustly detect these sig-
 380 nals associated with emissions of this magnitude. The linkage between observed enhance-
 381 ments and emissions depends on atmospheric conditions, so this detection threshold could
 382 be larger or smaller with variability in the atmosphere.

383 The average area of the grid cells contributing 50% of enhancement for the peaks
 384 in the features is $2.5 \pm 1 \text{ km}^2$. Comparatively, the average total flux field for the recep-
 385 tors is $614 \pm 243 \text{ km}^2$, and setting the threshold value to just the top 90% of the enhance-
 386 ment results in an average area of $35 \pm 21 \text{ km}^2$. Comparing the Cropland Data Layer to
 387 satellite imagery of the LMRB, the typical field size is $\sim 0.25 \text{ km}^2$, so peak enhancements
 388 can be attributed to an area equal to approximately 10 fields. Halving our grid resolu-
 389 tion to 0.01° in latitude and longitude, we find the result is consistent, with an average
 390 area of $2.5 \pm 1.5 \text{ km}^2$ and average flux of $0.023 \pm 0.015 \mu\text{mol m}^{-2} \text{s}^{-1}$ from the 50% thresh-
 391 old cells. Further reducing the resolution to 0.02° , the average area is $5.9 \pm 5.6 \text{ km}^2$ and

392 average flux is $0.019 \pm 0.017 \mu\text{mol m}^{-2} \text{s}^{-1}$, as each grid cell is roughly 4.2 km^2 , larger
393 than the 2.5 km^2 threshold area from the finer resolutions. The winds during the 05/02
394 transects were relatively steady and stable, resulting in narrow cones of particle trajec-
395 tories from the west, resulting in spatial extents of $7 \pm 2.5 \text{ km}$ in longitude and 1.3 ± 0.4
396 km in latitude for the peak enhancements. This inversion approach is intended to high-
397 light near-field local enhancements, and is not evaluating fluxes for the entire region. In
398 the a-posteriori grids, typically 70% of the grid cells were below the mean flux value, and
399 $\sim 2\%$ of the grid cells had negative fluxes. These fluxes are not designed to be represen-
400 tative of absolute values, but by comparing the shoulders of the plume to points above
401 the background we can attribute and identify the spatial scales and magnitudes of the
402 local enhancements.

403 **4 Implications**

404 Observed N_2O and CO_2 emissions from two productive fertilizer plants agree with
405 reported emissions, showing no evidence that emissions of these greenhouse gases are under-
406 or over-estimated in self-reporting. Our observed emissions of CH_4 from the two plants,
407 however, are greatly in excess of reported emissions, a phenomenon observed in other
408 fertilizer plants in the country (Zhou et al., 2019). Though emissions exceeding expect-
409 ation by multiple orders of magnitude may appear to be unrealistic, these emissions im-
410 ply a fugitive emission rate of $\sim 1\%$, a leakage rate consistent with observations from other
411 parts of the natural gas supply chain (Schwietzke et al., 2014). Although the observed
412 emissions are orders of magnitude higher than expected, the increased CH_4 emissions
413 do not significantly impact the overall footprint of the fertilizer plants, corresponding
414 to a 0.9% increase in total CO_2e emissions for Plant 1 and a 0.2% increase for Plant 2.
415 The large emissions of CO_2 and N_2O dominate any additional fugitive CH_4 emissions.
416 The fugitive CH_4 emissions may be modest in this case, but it is an addressable emis-
417 sions source and is under-estimated in current CH_4 inventories, thus representing another
418 discrepancy in inventory representation of CH_4 emissions.

419 Regional sampling of the LMRB enabled the investigation of emissions at a unique
420 spatial scale. We observed significant variability in N_2O emissions in the various sub-
421 regions sampled. Though the emissions magnitude and variability we observed is con-
422 sistent with flux chamber measurements, we might have expected less variability in the
423 regional flights that integrate over many fields with different crops and farming practices.

424 Considering the variability observed, soil moisture and crop type proved to be the strongest
425 emergent predictors of emissions. This suggests knowing the crop (and inherently thus
426 the soil type and fertilizer practice) combined with soil moisture can predict N₂O vari-
427 ability at 100 km scales, and highlights the role of soil moisture in predicting N₂O flux.
428 Future work evaluating how process-based models predict N₂O emissions to vary in this
429 domain will enable evaluation of process representations on regional spatial scales. Com-
430 paring emissions from plants to those from cropped soils, we observe 521.4 ± 92.8 kg/hr
431 of N₂O from the two fertilizer plants (averaging the two days for Plant 1). From soils
432 we observe around 15000 ± 7000 kg/hr of N₂O from a combined 92000 km² of area. This
433 value provides a snapshot of our domain at time of measurement, given how important
434 seasonality and spatial variability are to N₂O emissions from soil, and is not represen-
435 tative of larger trends, while the hourly plant emissions can be reasonably extrapolated.

436 We also assess our observed N₂O concentrations to define the ability of this type
437 of sampling to distinguish field-scale emissions, a critical spatial extent in-between the
438 facility-level analysis provided by the point-source quantification and the regional fluxes
439 from the mass balance calculations. We find that 50% of the total peak enhancement
440 in local features comes from areas with an average size of 2.5 ± 1 km² and average flux
441 magnitude of 0.026 ± 0.01 $\mu\text{mol m}^{-2} \text{s}^{-1}$. These suggests this method can potentially be
442 used to compare crop-management practices occurring on those spatial-scales, such as
443 no-till farming and/or different cover crops, to better assess the atmospheric impact from
444 different practices.

445 5 Conclusions

446 This work highlights the capability of continuous airborne observations to quan-
447 tify atmospheric greenhouse gas emissions from agricultural activity. We report green-
448 house gas emissions from two productive fertilizer plants with large production capac-
449 ity of ammonia and nitric acid and find good agreement with GHGRP-reported emis-
450 sions and observed N₂O and CO₂ emission rates. Observed CH₄ emissions are several
451 orders of magnitude higher, and suggest a natural gas leakage rate of $\sim 1\%$. Replacing
452 GHGRP-reported values with the observed emissions raises the CH₄ fractional contri-
453 bution to total plant emissions by a factor of 100, but the overall footprint of the facil-
454 ities is not substantially increased as the total footprint is dominated by reported N₂O
455 and CO₂ emissions.

456 We quantify regional N₂O fluxes using the mass balance technique, the first exam-
457 ple of this approach to agricultural N₂O emissions, demonstrating proof-of-concept. We
458 find fluxes on the order of 1.0 ± 0.7 g N₂O-N ha⁻¹ hr⁻¹, with large variability between
459 regions. We investigate relationships between emissions and several factors known to im-
460 pact N₂O: crop type, nitrogen from fertilizer application, soil moisture, and soil temper-
461 ature. For our flights we find the strongest predictors of N₂O emissions are soil mois-
462 ture, soybean area, cotton area, and rice area. Soil temperature and annual applied fer-
463 tilizer appear less predictive. The emission fluxes are broadly consistent with fluxes re-
464 ported in literature. Our method encompasses all emissions from the agricultural regions,
465 with total areas ranging from 5000 to 37000 km².

466 We estimate relative flux magnitudes and areas at local farm-level spatial scales
467 using a Bayesian inversion approach and the STILT model. We find an average flux of
468 0.026 ± 0.01 μmol m⁻² s⁻¹ (26 ± 10 g N₂O-N ha⁻¹ hr⁻¹) from an average area of 2.5 ± 1
469 km² is responsible for 50% of the total peak enhancement in a local N₂O feature. This
470 highlights the possibility to use airborne sampling to distinguish emission differences at
471 these spatial scales.

472 Future studies would benefit from observations of more fertilizer plants. Direct knowl-
473 edge of a facility's production rate would help reduce variability in scaling from annual
474 to hourly emissions, though that information may not be easily available. Comparing
475 the results of these flights with output from a process-based model for May 2017 in the
476 region of interest would allow direct comparison with expected N₂O fluxes as well as eval-
477 uation of the model's predicted sensitivity to underlying variables such as applied fer-
478 tilizer, soil moisture, or soil temperature. Another potential analysis would be compar-
479 ing the fluxes with measurements from an eddy covariance tower with appropriate foot-
480 print sizes. The type of airborne observations presented here could potentially be used
481 to assess the efficiency of various management practices by farms, evaluating if whole
482 field emissions vary depending on specific practices.

483 **Acknowledgments**

484 We thank Scientific Aviation for helping collect this data and Aerodyne Research Inc.
485 for their instrument-related guidance. This material is based partly upon work supported
486 by the National Science Foundation under Grant No. 1650682 and The University of Michi-
487 gan. The data is available at:

488 Kort E.A., Gvakharia A., Smith M.L., Conley S. Airborne Data from the Fertil-
 489 izer Emissions Airborne Study (FEAST). Nitrous Oxide, Carbon Dioxide, Carbon Monox-
 490 ide, Methane, Ozone, Water Vapor, and meteorological variables over the Mississippi River
 491 Valley [Data set]. University of Michigan Deep Blue Data Repository. <https://doi.org/10.7302/Z2XK8CRG>

492 References

- 493 Benjamin, S. G., Weygandt, S. S., Brown, J. M., Hu, M., Alexander, C. R.,
 494 Smirnova, T. G., ... others (2016). A north american hourly assimilation
 495 and model forecast cycle: The rapid refresh. *Monthly Weather Review*, *144*(4),
 496 1669–1694.
- 497 Brown, L., Armstrong Brown, S., Jarvis, S. C., Syed, B., Goulding, K. W. T.,
 498 Phillips, V. R., ... Pain, B. F. (2001). An inventory of nitrous oxide emissions
 499 from agriculture in the UK using the IPCC methodology: emission estimate,
 500 uncertainty and sensitivity analysis. *Atmospheric Environment*, *35*, 1439-1449.
 501 doi: 10.1016/S1352-2310(00)00361-7
- 502 Butterbach-Bahl, K., Baggs, E. M., Dannenmann, M., Kiese, R., & Zechmeister-
 503 Boltenstern, S. (2013, Jul 05). Nitrous oxide emissions from soils: how well do
 504 we understand the processes and their controls? *Philosophical Transactions of*
 505 *the Royal Society B: Biological Sciences*, *368*(1621), 20130122. Retrieved from
 506 <https://doi.org/10.1098/rstb.2013.0122> doi: 10.1098/rstb.2013.0122
- 507 Cao, P., Lu, C., & Yu, Z. (2017). *Agricultural nitrogen fertilizer uses in the con-*
 508 *tinental U.S. during 1850–2015: a set of gridded time-series data* [data set].
 509 PANGAEA. Retrieved from <https://doi.org/10.1594/PANGAEA.883585>
 510 (Supplement to: Cao, P et al. (in review): Historical Nitrogen Fertilizer Use
 511 in Agricultural Ecosystem of the Continental U.S. during 1850-2015: Appli-
 512 cation rate, Timing, and Fertilizer Types. Earth System Science Data) doi:
 513 10.1594/PANGAEA.883585
- 514 Cao, P., Lu, C., & Yu, Z. (2018). Historical nitrogen fertilizer use in agricultural
 515 ecosystems of the contiguous United States during 1850–2015: application rate,
 516 timing, and fertilizer types. *Earth System Science Data*, *10*(2), 969–984. Re-
 517 trieved from <https://www.earth-syst-sci-data.net/10/969/2018/> doi:
 518 10.5194/essd-10-969-2018
- 519 Chen, Z., Griffis, T. J., Millet, D. B., Wood, J. D., Lee, X., Baker, J. M., ... Wells,

- 520 K. C. (2016). Partitioning N₂O emissions within the U.S. Corn Belt using an
521 inverse modeling approach. *Global Biogeochemical Cycles*, *30*(8), 1192–1205.
522 Retrieved from <http://dx.doi.org/10.1002/2015GB005313> (2015GB005313)
523 doi: 10.1002/2015GB005313
- 524 Conley, S., Faloon, I., Mehrotra, S., Suard, M., Lenschow, D. H., Sweeney, C.,
525 ... Schnell, R. (2017). Application of Gauss's theorem to quantify lo-
526 calized surface emissions from airborne measurements of wind and trace
527 gases. *Atmospheric Measurement Techniques*, *10*(9), 3345–3358. Re-
528 trieved from <https://www.atmos-meas-tech.net/10/3345/2017/> doi:
529 10.5194/amt-10-3345-2017
- 530 Conley, S. A., Faloon, I. C., Lenschow, D. H., Karion, A., & Sweeney, C. (2014).
531 A low-cost system for measuring horizontal winds from single-engine air-
532 craft. *Journal of Atmospheric and Oceanic Technology*, *31*(6), 1312–1320.
533 Retrieved from <https://doi.org/10.1175/JTECH-D-13-00143.1> doi:
534 10.1175/JTECH-D-13-00143.1
- 535 Del Grosso, S., J Parton, W., Mosier, A., K Walsh, M., S Ojima, D., & E Thornton,
536 P. (2006, 07). DAYCENT national-scale simulations of nitrous oxide emissions
537 from cropped soils in the United States. *Journal of Environmental Quality*, *35*,
538 1451–60.
- 539 Dlugokencky, E. J., Myers, R. C., Lang, P. M., Masarie, K. A., Crotwell, A. M.,
540 Thoning, K. W., ... Steele, L. P. (2005). Conversion of NOAA atmo-
541 spheric dry air CH₄ mole fractions to a gravimetrically prepared standard
542 scale. *Journal of Geophysical Research: Atmospheres*, *110*(D18). Retrieved
543 from [https://agupubs.onlinelibrary.wiley.com/doi/abs/10.1029/](https://agupubs.onlinelibrary.wiley.com/doi/abs/10.1029/2005JD006035)
544 [2005JD006035](https://agupubs.onlinelibrary.wiley.com/doi/abs/10.1029/2005JD006035) doi: 10.1029/2005JD006035
- 545 Dobbie, K. E., McTaggart, I. P., & Smith, K. A. (1999). Nitrous oxide emissions
546 from intensive agricultural systems: Variations between crops and seasons,
547 key driving variables, and mean emission factors. *Journal of Geophysical*
548 *Research: Atmospheres*, *104*(D21), 26891–26899. Retrieved from [https://](https://agupubs.onlinelibrary.wiley.com/doi/abs/10.1029/1999JD900378)
549 agupubs.onlinelibrary.wiley.com/doi/abs/10.1029/1999JD900378 doi:
550 10.1029/1999JD900378
- 551 EFMA. (2000). *Production of nitric acid. booklet no. 2 of 8: Best available tech-*
552 *niques for pollution control in the european fertilizer industry.* Ave. E van

- 553 Nieuwenhuysse 4, B-1160 Brussels, Belgium: European Fertilizer Manufacturers
 554 Association. [http://fertilizerseurope.com/fileadmin/user_upload/
 555 publications/technical_publications/BATs/Booklet_2_final.pdf](http://fertilizerseurope.com/fileadmin/user_upload/publications/technical_publications/BATs/Booklet_2_final.pdf).
- 556 Ehrhardt, F., Soussana, J.-F., Bellocchi, G., Grace, P., McAuliffe, R., Recous, S., ...
 557 Zhang, Q. (2017). Assessing uncertainties in crop and pasture ensemble model
 558 simulations of productivity and N₂O emissions. *Global Change Biology*, *24*(2),
 559 e603-e616. Retrieved from [https://onlinelibrary.wiley.com/doi/abs/
 560 10.1111/gcb.13965](https://onlinelibrary.wiley.com/doi/abs/10.1111/gcb.13965) doi: 10.1111/gcb.13965
- 561 EPA. (2017). *Greenhouse Gas Reporting Program (GHGRP) FLIGHT Data system*.
 562 <http://ghgdata.epa.gov/ghgp/>. US Environmental Protection Agency.
- 563 Erisman, J., Sutton, M., Galloway, J., Klimont, Z., & Winiwarter, W. (2008, Oc-
 564 tober). How a century of ammonia synthesis changed the world. *Nature
 565 Geoscience*, *1*(10), 636–639. Retrieved from [http://pure.iiasa.ac.at/id/
 566 eprint/8475/](http://pure.iiasa.ac.at/id/eprint/8475/) doi: 10.1038/ngeo325
- 567 FAO. (2017). *World fertilizer trends and outlook to 2020*.
- 568 Fossum, J.-P. (2014). *Calculation of carbon footprint of fertilizer production*.
 569 [http://www.yara.com/doc/122597_2013_Carbon_footprintof_AN_Method
 570 _of_calculation.pdf](http://www.yara.com/doc/122597_2013_Carbon_footprintof_AN_Method_of_calculation.pdf).
- 571 Gellings, C. W., & Parmenter, K. E. (2016). Energy efficiency in fertilizer produc-
 572 tion and use. *Efficient Use and Conservation of Energy; Gellings, CW, Ed.;
 573 Encyclopedia of Life Support Systems*, 123–136.
- 574 Gerbig, C., Lin, J. C., Wofsy, S. C., Daube, B. C., Andrews, A. E., Stephens, B. B.,
 575 ... Grainger, C. A. (2003). Toward constraining regional-scale fluxes of CO₂
 576 with atmospheric observations over a continent: 2. analysis of COBRA data using
 577 a receptor-oriented framework. *Journal of Geophysical Research: Atmospheres*,
 578 *108*(D24). Retrieved from [https://agupubs.onlinelibrary.wiley.com/
 579 doi/abs/10.1029/2003JD003770](https://agupubs.onlinelibrary.wiley.com/doi/abs/10.1029/2003JD003770) doi: 10.1029/2003JD003770
- 580 Grant, R., Pattey, E., Goddard, T., Kryzanowski, L., & Puurveen, H. (2006,
 581 01). Modeling the effects of fertilizer application rate on nitrous oxide
 582 emissions. *Soil Science Society of America Journal*, *70*, 235-248. doi:
 583 10.2136/sssaj2005.0104
- 584 Griffis, T. J., Chen, Z., Baker, J. M., Wood, J. D., Millet, D. B., Lee, X., ... Turner,
 585 P. A. (2017). Nitrous oxide emissions are enhanced in a warmer and wetter

- 586 world. *Proceedings of the National Academy of Sciences*, 114(45), 12081–
587 12085. Retrieved from <http://www.pnas.org/content/114/45/12081> doi:
588 10.1073/pnas.1704552114
- 589 Gvakharia, A., Kort, E. A., Smith, M. L., & Conley, S. (2018). Testing and eval-
590 uation of a new airborne system for continuous N₂O, CO₂, CO, and H₂O mea-
591 surements: the Frequent Calibration High-performance Airborne Observation
592 System (FCHAOS). *Atmospheric Measurement Techniques*, 11(11), 6059–6074.
593 Retrieved from <https://www.atmos-meas-tech.net/11/6059/2018/> doi:
594 10.5194/amt-11-6059-2018
- 595 Heimann, D. C., Holmes Jr., R. R., & Harris, T. E. (2018). *Flooding in the southern*
596 *Midwestern United States, April–May 2017* (Tech. Rep.). Reston, VA: USGS.
597 Retrieved from <http://pubs.er.usgs.gov/publication/ofr20181004> (Re-
598 port)
- 599 Karion, A., Sweeney, C., Kort, E. A., Shepson, P. B., Brewer, A., Cambaliza, M.,
600 ... Tans, P. (2015). Aircraft-based estimate of total methane emissions from
601 the Barnett Shale region. *Environmental Science & Technology*, 49(13), 8124–
602 8131. Retrieved from <https://doi.org/10.1021/acs.est.5b00217> (PMID:
603 26148550) doi: 10.1021/acs.est.5b00217
- 604 Karion, A., Sweeney, C., Wolter, S., Newberger, T., Chen, H., Andrews, A., ...
605 Tans, P. (2013). Long-term greenhouse gas measurements from aircraft. *At-*
606 *mospheric Measurement Techniques*, 6(3), 511–526. Retrieved from [https://](https://www.atmos-meas-tech.net/6/511/2013/)
607 www.atmos-meas-tech.net/6/511/2013/ doi: 10.5194/amt-6-511-2013
- 608 Kort, E., Gvakharia, A., Smith, M., & Conley, S. (2018). *Airborne Data from the*
609 *Fertilizer Emissions Airborne Study (FEAST). Nitrous Oxide, Carbon Dioxide,*
610 *Carbon Monoxide, Methane, Ozone, Water Vapor, and meteorological variables*
611 *over the Mississippi River Valley* [data set]. University of Michigan Deep Blue
612 Data Repository. Retrieved from <https://doi.org/10.7302/Z2XK8CRG> doi:
613 10.7302/Z2XK8CRG
- 614 Kort, E. A., Smith, M. L., Murray, L. T., Gvakharia, A., Brandt, A. R., Peischl, J.,
615 ... Travis, K. (2016). Fugitive emissions from the Bakken shale illustrate role
616 of shale production in global ethane shift. *Geophysical Research Letters*, 43(9),
617 4617–4623. Retrieved from <http://dx.doi.org/10.1002/2016GL068703>
618 (2016GL068703) doi: 10.1002/2016GL068703

- 619 Lemke, R., Liu, L., Baron, V., Malhi, S., & Farrell, R. (2018). Effect of crop
620 and residue type on nitrous oxide emissions from rotations in the semi-
621 arid Canadian prairies. *Canadian Journal of Soil Science*, 98(3), 508-
622 518. Retrieved from <https://doi.org/10.1139/cjss-2018-0001> doi:
623 10.1139/cjss-2018-0001
- 624 Lin, J. C., Gerbig, C., Wofsy, S. C., Andrews, A. E., Daube, B. C., Davis, K. J., &
625 Grainger, C. A. (2003). A near-field tool for simulating the upstream influence
626 of atmospheric observations: The stochastic time-inverted lagrangian trans-
627 port (stilt) model. *Journal of Geophysical Research: Atmospheres*, 108(D16).
628 Retrieved from [https://agupubs.onlinelibrary.wiley.com/doi/abs/
629 10.1029/2002JD003161](https://agupubs.onlinelibrary.wiley.com/doi/abs/10.1029/2002JD003161) doi: 10.1029/2002JD003161
- 630 Linn, D., & Doran, J. (1984, 11). Effect of water-filled pore space on carbon dioxide
631 and nitrous oxide production in tilled and nontilled soils¹. *Soil Science Society
632 of America Journal*, 48. doi: 10.2136/sssaj1984.03615995004800060013x
- 633 Lu, C., & Tian, H. (2017). Global nitrogen and phosphorus fertilizer use
634 for agriculture production in the past half century: shifted hot spots and
635 nutrient imbalance. *Earth System Science Data*, 9(1), 181–192. Re-
636 trieved from <https://www.earth-syst-sci-data.net/9/181/2017/> doi:
637 10.5194/essd-9-181-2017
- 638 Lund, D., J.D. Atwood, J. B., Benson, J., Goebel, J., Ingram, K., Johnson, M.-V.,
639 ... Plotkin., S. (2013). *Assessment of the effects of conservation practices
640 on cultivated cropland in the Lower Mississippi River Basin* (Tech. Rep.).
641 Washington, DC: USDA NRCS.
- 642 Marinho, E. V. A., DeLaune, R. D., & Lindau, C. W. (2004). Nitrous oxide flux
643 from soybeans grown on Mississippi alluvial soil. *Communications in Soil Sci-
644 ence and Plant Analysis*, 35(1-2), 1-8. Retrieved from [https://doi.org/10
645 .1081/CSS-120027630](https://doi.org/10.1081/CSS-120027630) doi: 10.1081/CSS-120027630
- 646 Mehrotra, S., Faloona, I., Suard, M., Conley, S., & Fischer, M. L. (2017, Nov).
647 Airborne Methane Emission Measurements for Selected Oil and Gas Facilities
648 Across California. *Environ. Sci. Technol.*, 51(21), 12981–12987.
- 649 Mesinger, F., DiMego, G., Kalnay, E., Mitchell, K., Shafran, P. C., Ebisuzaki,
650 W., ... Shi, W. (2006). North American Regional Reanalysis. *Bulletin
651 of the American Meteorological Society*, 87(3), 343-360. Retrieved from

- 652 <https://doi.org/10.1175/BAMS-87-3-343> (NCEP Reanalysis data provided
653 by the NOAA/OAR/ESRL PSD, Boulder, Colorado, USA, from their
654 Web site at <https://www.esrl.noaa.gov/psd/>) doi: 10.1175/BAMS-87-3-343
- 655 Monni, S., Perälä, P., & Regina, K. (2007, May 01). Uncertainty in agricultural CH₄
656 and N₂O emissions from Finland – possibilities to increase accuracy in emis-
657 sion estimates. *Mitigation and Adaptation Strategies for Global Change*, 12(4),
658 545–571. Retrieved from <https://doi.org/10.1007/s11027-006-4584-4>
659 doi: 10.1007/s11027-006-4584-4
- 660 Myhre, G., Shindell, D., Bron, F.-M., Collins, W., Fuglestvedt, J., Huang, J.,
661 ... Zhang, H. (2013). Anthropogenic and natural radiative forcing. In
662 T. F. Stocker et al. (Eds.), *Climate change 2013: The physical science basis.*
663 *contribution of working group i to the fifth assessment report of the intergov-*
664 *ernmental panel on climate change* (pp. 659–740). Cambridge, UK: Cambridge
665 University Press. doi: 10.1017/CBO9781107415324.018
- 666 Nevison, C., Andrews, A., Thoning, K., Dlugokencky, E., Sweeney, C., Miller,
667 S., ... Nehrkorn, T. (2018). Nitrous oxide emissions estimated with the
668 CarbonTrackerLagrange North American Regional Inversion Framework.
669 *Global Biogeochemical Cycles*, 32(3), 463-485. Retrieved from [https://](https://agupubs.onlinelibrary.wiley.com/doi/abs/10.1002/2017GB005759)
670 agupubs.onlinelibrary.wiley.com/doi/abs/10.1002/2017GB005759 doi:
671 10.1002/2017GB005759
- 672 Nutrien. (2018). *Nutrien 2018 Fact Book*. [https://www.nutrien.com/sites/](https://www.nutrien.com/sites/default/files/uploads/2018-01/Nutrien%20Fact%20Book%202018.1.pdf)
673 [default/files/uploads/2018-01/Nutrien%20Fact%20Book%202018.1.pdf](https://www.nutrien.com/sites/default/files/uploads/2018-01/Nutrien%20Fact%20Book%202018.1.pdf).
674 Saskatoon, Saskatchewan, Canada.
- 675 O'Neill, P., Chan, S., Njoku, E., Jackson, T., & Bindlish, R. (2018). *SMAP En-*
676 *hanced L3 Radiometer Global Daily 9 km EASE-Grid Soil Moisture, Version*
677 *2 [L3, Passive, Day]*. Boulder, Colorado USA. ([Accessed 10/31/2018]) doi:
678 10.5067/RFKIZ5QY5ABN
- 679 Padgitt, M., Newton, D., Penn, R., & Sandretto, C. (2000, September). *Pro-*
680 *duction Practices for Major Crops in U.S. Agriculture, 1990-97* (Statistical
681 Bulletin No. 262287). United States Department of Agriculture, Economic
682 Research Service. Retrieved from [https://ideas.repec.org/p/ags/uerssb/](https://ideas.repec.org/p/ags/uerssb/262287.html)
683 [262287.html](https://ideas.repec.org/p/ags/uerssb/262287.html)
- 684 Parkin, T., Venterea, R., & Hargreaves, S. (2012, 05). Calculating the detection lim-

- 685 its of chamber-based soil greenhouse gas flux measurements. *Journal of envi-*
 686 *ronmental quality*, 41, 705-15. doi: 10.2134/jeq2011.0394
- 687 Parkin, T. B., & Kaspar, T. C. (2006). Nitrous oxide emissions from corn-soybean
 688 systems in the Midwest. *J. Environ. Qual.*, 35(4), 1496–1506.
- 689 Pattey, E., Blackburn, L. G., Strachan, I. B., Desjardins, R., & Dow, D. (2008).
 690 Spring thaw and growing season N₂O emissions from a field planted with
 691 edible peas and a cover crop. *Canadian Journal of Soil Science*, 88(2),
 692 241-249. Retrieved from <https://doi.org/10.4141/CJSS06035> doi:
 693 10.4141/CJSS06035
- 694 Peischl, J., Ryerson, T. B., Aikin, K. C., Gouw, J. A., Gilman, J. B., Holloway, J. S.,
 695 ... Parrish, D. D. (2015). Quantifying atmospheric methane emissions from
 696 the Haynesville, Fayetteville, and northeastern Marcellus shale gas production
 697 regions. *Journal of Geophysical Research: Atmospheres*, 120(5), 2119-2139.
 698 Retrieved from [https://agupubs.onlinelibrary.wiley.com/doi/abs/](https://agupubs.onlinelibrary.wiley.com/doi/abs/10.1002/2014JD022697)
 699 10.1002/2014JD022697 doi: 10.1002/2014JD022697
- 700 Rapson, T. D., & Dacres, H. (2014). Analytical techniques for measuring nitrous
 701 oxide. *TrAC Trends in Analytical Chemistry*, 54, 65 - 74. Retrieved from
 702 <http://www.sciencedirect.com/science/article/pii/S0165993613002574>
 703 doi: <https://doi.org/10.1016/j.trac.2013.11.004>
- 704 Ravishankara, A. R., Daniel, J. S., & Portmann, R. W. (2009). Nitrous oxide (N₂O):
 705 The dominant ozone-depleting substance emitted in the 21st century. *Sci-*
 706 *ence*, 326(5949), 123–125. Retrieved from [http://science.sciencemag.org/](http://science.sciencemag.org/content/326/5949/123)
 707 [content/326/5949/123](http://science.sciencemag.org/content/326/5949/123) doi: 10.1126/science.1176985
- 708 Reay, D. S., Davidson, E. A., Smith, K. A., Smith, P., Melillo, J. M., Dentener,
 709 F., & Crutzen, P. J. (2012, may). Global agriculture and nitrous ox-
 710 ide emissions. *Nature Climate Change*, 2(6), 410–416. Retrieved from
 711 <https://doi.org/10.1038/nclimate1458> doi: 10.1038/nclimate1458
- 712 Rodgers, C. D. (2000). *Inverse methods for atmospheric sounding: theory and prac-*
 713 *tice* (Vol. 2). World scientific.
- 714 Römkens, M., Selim, H., Scott, H., Phillips, R., & Whisler, F. (1986). Physical char-
 715 acteristics of soils in the Southern Region: Captina, Gigger, Grenada, Loring,
 716 Olivier and Sharkey series. *Southern Cooperative Series Bulletin*, 264.
- 717 Scaroni, A. E., Ye, S., Lindau, C. W., & Nyman, J. A. (2014, Jun 01). Nitrous

- 718 oxide emissions from soils in Louisiana's Atchafalaya River Basin. *Wetlands*,
719 *34*(3), 545–554. Retrieved from [https://doi.org/10.1007/s13157-014-0521-](https://doi.org/10.1007/s13157-014-0521-6)
720 [6](https://doi.org/10.1007/s13157-014-0521-6) doi: 10.1007/s13157-014-0521-6
- 721 Schindlbacher, A., Zechmeister-Boltenstern, S., & Butterbach-Bahl, K. (2004).
722 Effects of soil moisture and temperature on NO, NO₂, and N₂O emissions
723 from European forest soils. *Journal of Geophysical Research: Atmospheres*,
724 *109*(D17). Retrieved from [https://agupubs.onlinelibrary.wiley.com/](https://agupubs.onlinelibrary.wiley.com/doi/abs/10.1029/2004JD004590)
725 [doi/abs/10.1029/2004JD004590](https://doi.org/10.1029/2004JD004590) doi: 10.1029/2004JD004590
- 726 Schwarz, J. P., Holloway, J. S., Katich, J. M., McKeen, S., Kort, E. A., Smith,
727 M. L., ... Peischl, J. (2015). Black carbon emissions from the Bakken oil and
728 gas development region. *Environmental Science & Technology Letters*, *2*(10),
729 281–285. Retrieved from <https://doi.org/10.1021/acs.estlett.5b00225>
730 doi: 10.1021/acs.estlett.5b00225
- 731 Schwietzke, S., Griffin, W. M., Matthews, H. S., & Bruhwiler, L. M. (2014). Natural
732 gas fugitive emissions rates constrained by global atmospheric methane and
733 ethane. *Environmental science & technology*, *48*(14), 7714–7722.
- 734 Scott, H. D., Ferguson, J. A., Hanson, L., Fugitt, T., & Smith, E. (1998). *Agricultural water management in the Mississippi Delta Region of Arkansas*.
- 735
- 736 Selim, H., Davidoff, B., Fluhler, H., & Schulin, R. (1987). Variability of in situ mea-
737 sured mechanical impedance for a fragipan soil. *Soil science*, *144*(6), 442–452.
- 738 Smil, V. (2011). Nitrogen cycle and world food production. *World Agriculture*, *2*(1),
739 9–13.
- 740 Smith, K. A., Ball, T., Conen, F., Dobbie, K. E., Massheder, J., & Rey, A. (2003).
741 Exchange of greenhouse gases between soil and atmosphere: interactions of soil
742 physical factors and biological processes. *European Journal of Soil Science*,
743 *54*(4), 779–791. Retrieved from [https://onlinelibrary.wiley.com/doi/](https://onlinelibrary.wiley.com/doi/abs/10.1046/j.1351-0754.2003.0567.x)
744 [abs/10.1046/j.1351-0754.2003.0567.x](https://doi.org/10.1046/j.1351-0754.2003.0567.x) doi: 10.1046/j.1351-0754.2003.0567
745 .x
- 746 Smith, K. A., Thomson, P. E., Clayton, H., McTaggart, I. P., & Conen, F. (1998).
747 Effects of temperature, water content and nitrogen fertilisation on emissions
748 of nitrous oxide by soils. *Atmospheric Environment*, *32*(19), 3301 - 3309.
749 Retrieved from [http://www.sciencedirect.com/science/article/pii/](http://www.sciencedirect.com/science/article/pii/S1352231097004925)
750 [S1352231097004925](https://doi.org/10.1016/S1352-2310(97)00492-5) doi: [https://doi.org/10.1016/S1352-2310\(97\)00492-5](https://doi.org/10.1016/S1352-2310(97)00492-5)

- 751 Smith, M. L., Gvakharia, A., Kort, E. A., Sweeney, C., Conley, S. A., Faloona, I.,
752 ... Wolter, S. (2017). Airborne quantification of methane emissions over the
753 Four Corners Region. *Environmental Science & Technology*, 51(10), 5832-
754 5837. Retrieved from <https://doi.org/10.1021/acs.est.6b06107> (PMID:
755 28418663) doi: 10.1021/acs.est.6b06107
- 756 Smith, M. L., Kort, E. A., Karion, A., Sweeney, C., Herndon, S. C., & Yacov-
757 itch, T. I. (2015). Airborne ethane observations in the Barnett Shale:
758 Quantification of ethane flux and attribution of methane emissions. *En-
759 vironmental Science & Technology*, 49(13), 8158-8166. Retrieved from
760 <https://doi.org/10.1021/acs.est.5b00219> (PMID: 26148554) doi:
761 10.1021/acs.est.5b00219
- 762 Snipes, C. E., Evans, L. P., Poston, D. H., & Nichols, S. P. (2004). Agricultural
763 Practices of the Mississippi Delta. In *Water quality assessments in the missis-
764 sippi delta* (p. 43-60). American Chemical Society. Retrieved from [https://
765 pubs.acs.org/doi/abs/10.1021/bk-2004-0877.ch004](https://pubs.acs.org/doi/abs/10.1021/bk-2004-0877.ch004) doi: 10.1021/bk-2004-
766 -0877.ch004
- 767 Soane, B. (1990). The role of organic matter in soil compactibility: A review of some
768 practical aspects. *Soil and Tillage Research*, 16(1), 179 - 201. Retrieved from
769 <http://www.sciencedirect.com/science/article/pii/016719879090029D>
770 (A Tribute to Prof. IR. H. Kuipers) doi: <https://doi.org/10.1016/0167>
771 -1987(90)90029-D
- 772 Speight, J. (2007). Liquid fuels from natural gas. *Handbook of Alternative Fuel Tech-
773 nologies*, 153.
- 774 TFI. (2017). *2017 State of the Fertilizer Industry*. Washington, D.C..
- 775 Tian, H., Chen, G., Zhang, C., Liu, M., Sun, G., Chappelka, A., ... others (2012).
776 Century-scale responses of ecosystem carbon storage and flux to multiple
777 environmental changes in the southern United States. *Ecosystems*, 15(4),
778 674-694.
- 779 USDA. (2017). *USDA National Agricultural Statistics Service Cropland Data
780 Layer*. Published crop-specific data layer [Online]. Available at [https://
781 nassgeodata.gmu.edu/CropScape/](https://nassgeodata.gmu.edu/CropScape/). Last accessed October 2018. USDA-
782 NASS, Washington, DC.
- 783 USDA ARS. (2012). *Lower Mississippi River Basin* (Tech. Rep.). Washington,

- 784 DC: United States Department of Agriculture, Agricultural Research Service.
785 <https://www.ars.usda.gov/ARSUserFiles/np211/LMRBProposal.pdf>.
- 786 USDA ARS. (2014). *LMRB*. <https://l1tar.ars.usda.gov/sites/lmrbl/>.
- 787 USDA NASS. (2017a). *May 15, 2017 Crop Progress Report*. [https://](https://downloads.usda.library.cornell.edu/usda-esmis/files/8336h188j/k0698890n/wp988m39m/CropProg-05-15-2017.pdf)
788 [downloads.usda.library.cornell.edu/usda-esmis/files/8336h188j/](https://downloads.usda.library.cornell.edu/usda-esmis/files/8336h188j/k0698890n/wp988m39m/CropProg-05-15-2017.pdf)
789 [k0698890n/wp988m39m/CropProg-05-15-2017.pdf](https://downloads.usda.library.cornell.edu/usda-esmis/files/8336h188j/k0698890n/wp988m39m/CropProg-05-15-2017.pdf). USDA-NASS, Washing-
790 ton, DC.
- 791 USDA NASS. (2017b). *May 8, 2017 Crop Progress Report*. [https://downloads](https://downloads.usda.library.cornell.edu/usda-esmis/files/8336h188j/jw827d33p/kh04dr233/CropProg-05-08-2017.pdf)
792 [.usda.library.cornell.edu/usda-esmis/files/8336h188j/jw827d33p/](https://downloads.usda.library.cornell.edu/usda-esmis/files/8336h188j/jw827d33p/kh04dr233/CropProg-05-08-2017.pdf)
793 [kh04dr233/CropProg-05-08-2017.pdf](https://downloads.usda.library.cornell.edu/usda-esmis/files/8336h188j/jw827d33p/kh04dr233/CropProg-05-08-2017.pdf). USDA-NASS, Washington, DC.
- 794 USGS. (2018). *2018 Mineral Commodity Summaries, Nitrogen (Fixed)Ammonia*.
795 [https://minerals.usgs.gov/minerals/pubs/commodity/nitrogen/](https://minerals.usgs.gov/minerals/pubs/commodity/nitrogen/mcs-2018-nitro.pdf)
796 [mcs-2018-nitro.pdf](https://minerals.usgs.gov/minerals/pubs/commodity/nitrogen/mcs-2018-nitro.pdf).
- 797 USGS. (2019). *2016 Minerals Yearbook, Nitrogen (Advanced Release)*. [https://](https://prd-wret.s3-us-west-2.amazonaws.com/assets/palladium/production/atoms/files/myb1-2016-nitro.pdf)
798 [prd-wret.s3-us-west-2.amazonaws.com/assets/palladium/production/](https://prd-wret.s3-us-west-2.amazonaws.com/assets/palladium/production/atoms/files/myb1-2016-nitro.pdf)
799 [atoms/files/myb1-2016-nitro.pdf](https://prd-wret.s3-us-west-2.amazonaws.com/assets/palladium/production/atoms/files/myb1-2016-nitro.pdf).
- 800 Vaughn, T. L., Bell, C. S., Yacovitch, T. I., Roscioli, J. R., Herndon, S. C., Conley,
801 S., ... Zimmerle, D. (2017, nov). Comparing facility-level methane emission
802 rate estimates at natural gas gathering and boosting stations. *Elem Sci Anth*,
803 5(0), 71. Retrieved from <https://doi.org/10.1525/elementa.257> doi:
804 10.1525/elementa.257
- 805 White, W., Anderson, J., Blumenthal, D., Husar, R., Gillani, N., Husar, J., & Wil-
806 son, W. (1976). Formation and transport of secondary air pollutants: ozone
807 and aerosols in the St. Louis urban plume. *Science*, 194(4261), 187–189. Re-
808 trieved from <http://science.sciencemag.org/content/194/4261/187> doi:
809 10.1126/science.959846
- 810 Zhou, X., Passow, F. H., Rudek, J., von Fisher, J. C., Hamburg, S. P., & Albertson,
811 J. D. (2019). Estimation of methane emissions from the us ammonia fertilizer
812 industry using a mobile sensing approach. *Elem Sci Anth*, 7(1).

Figure 1.

Author Manuscript

38
37
36
35
34
33
32
31

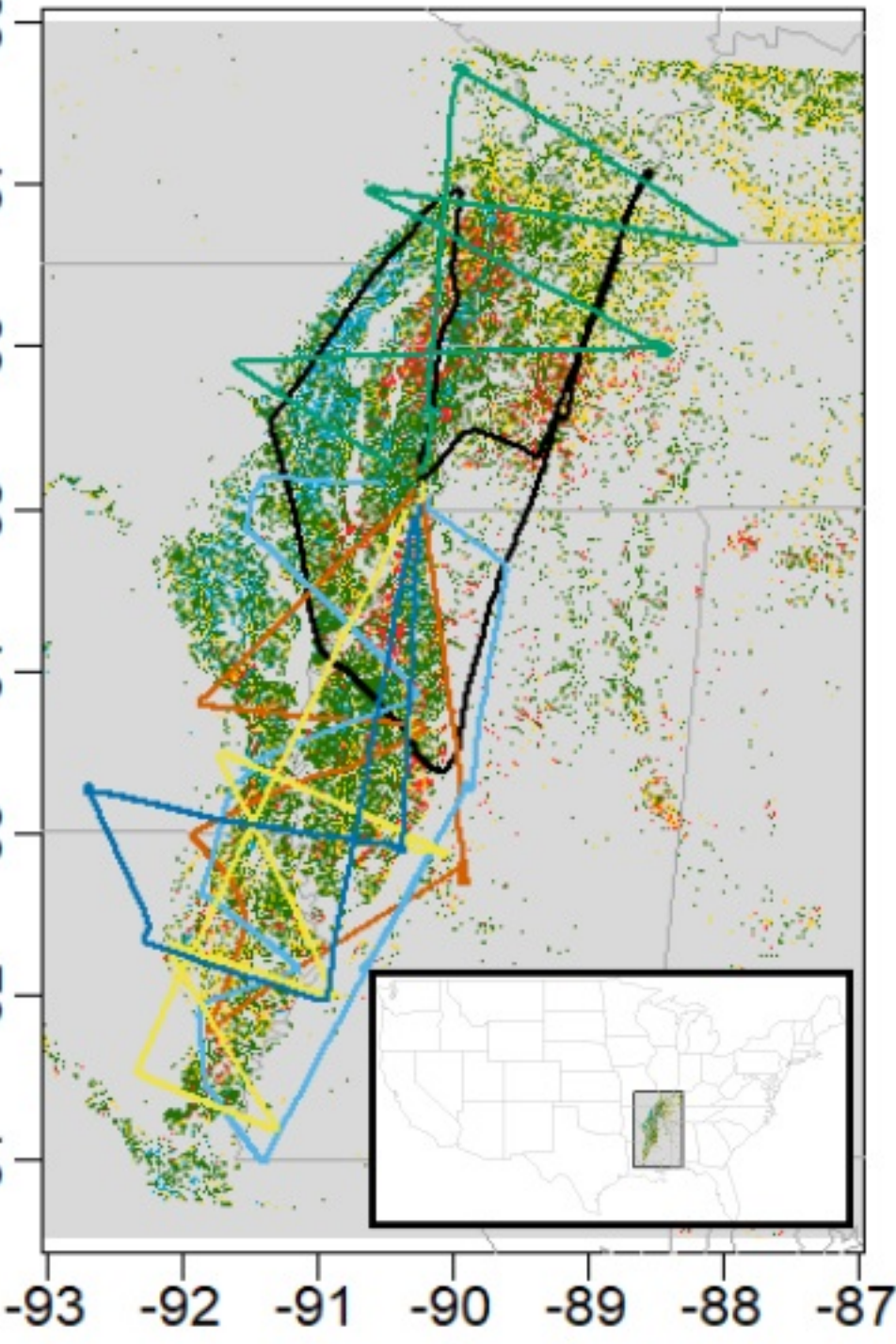


Figure 2.

Author Manuscript

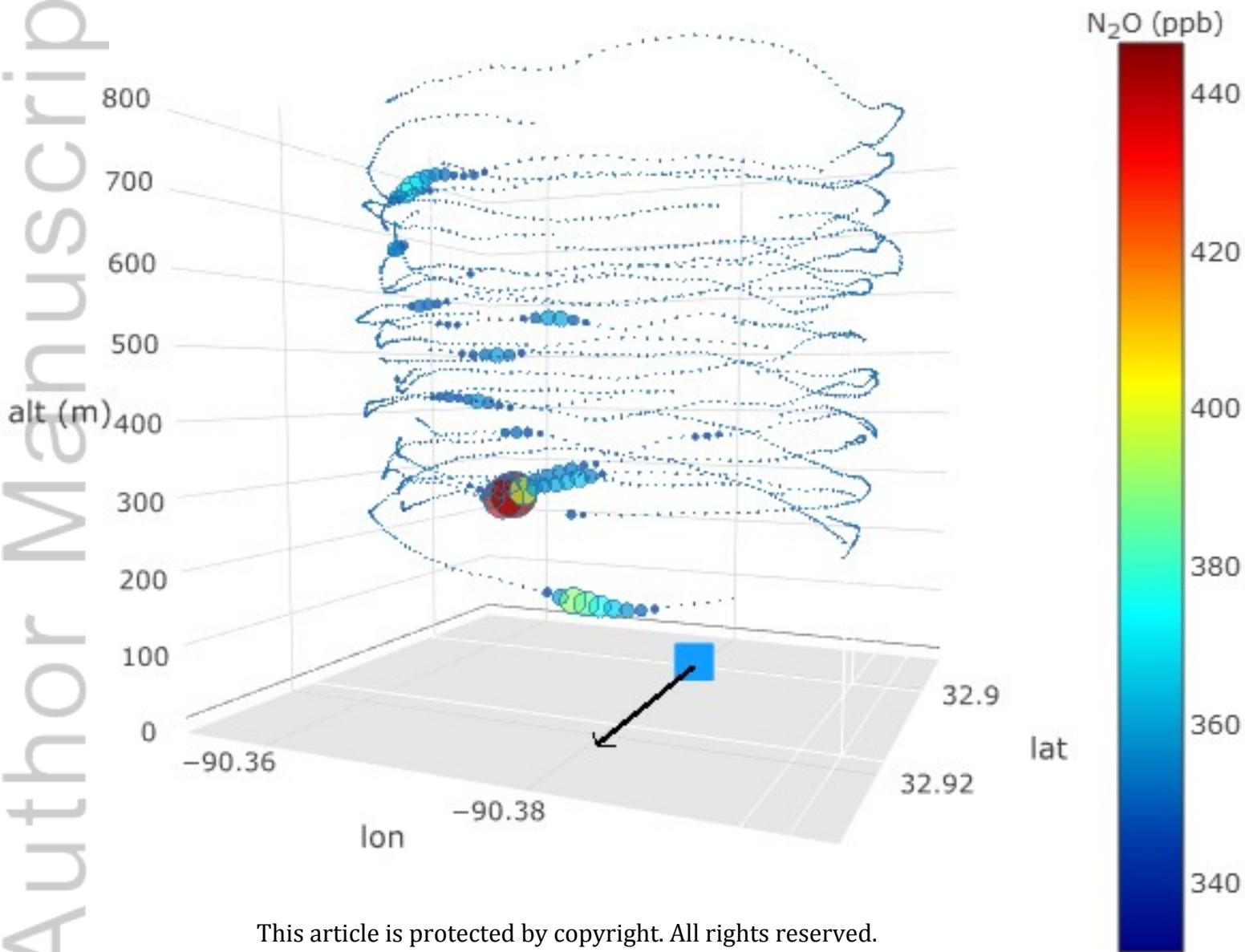


Figure 3.

Author Manuscript

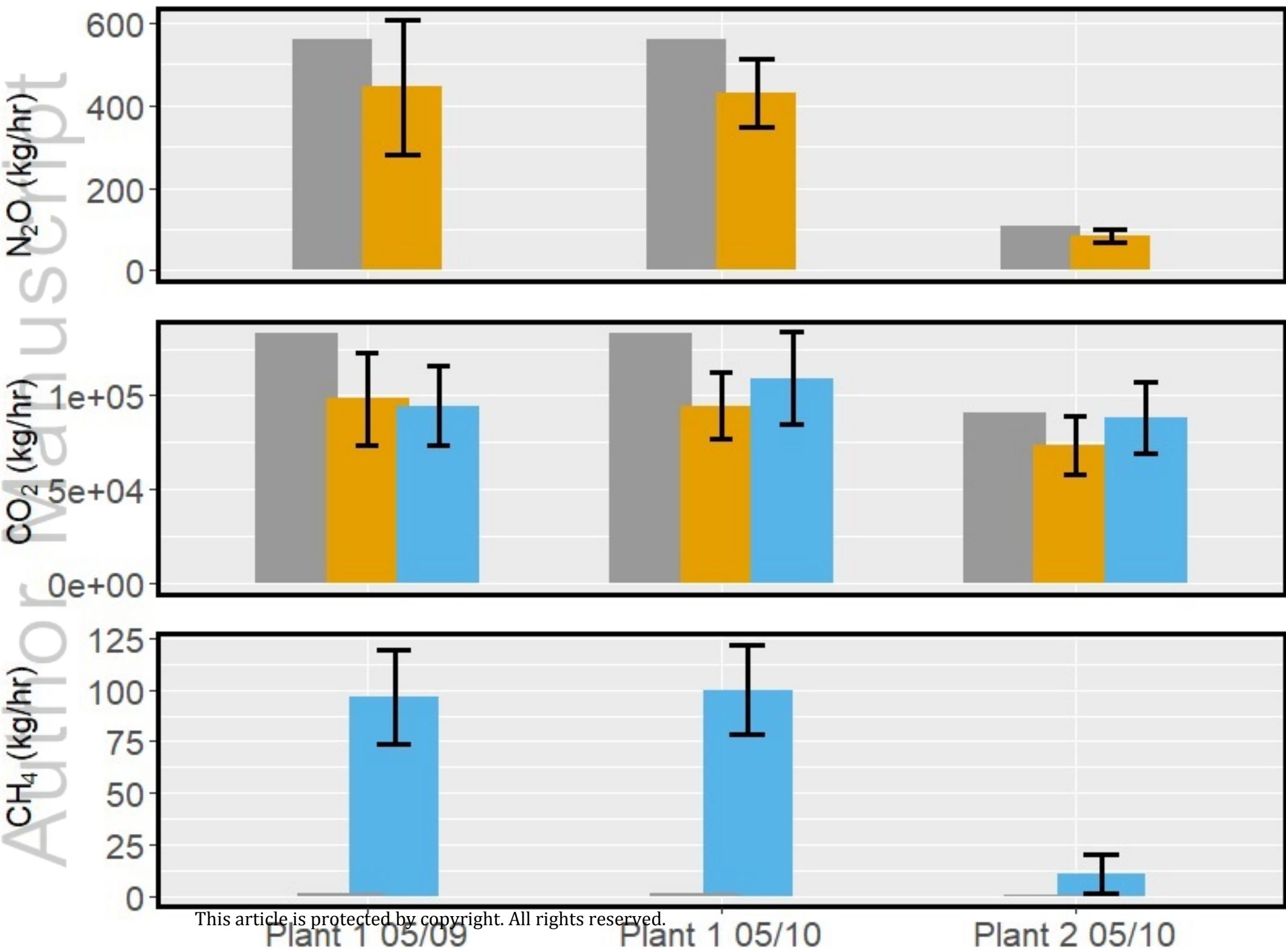


Figure 4.

Author Manuscript

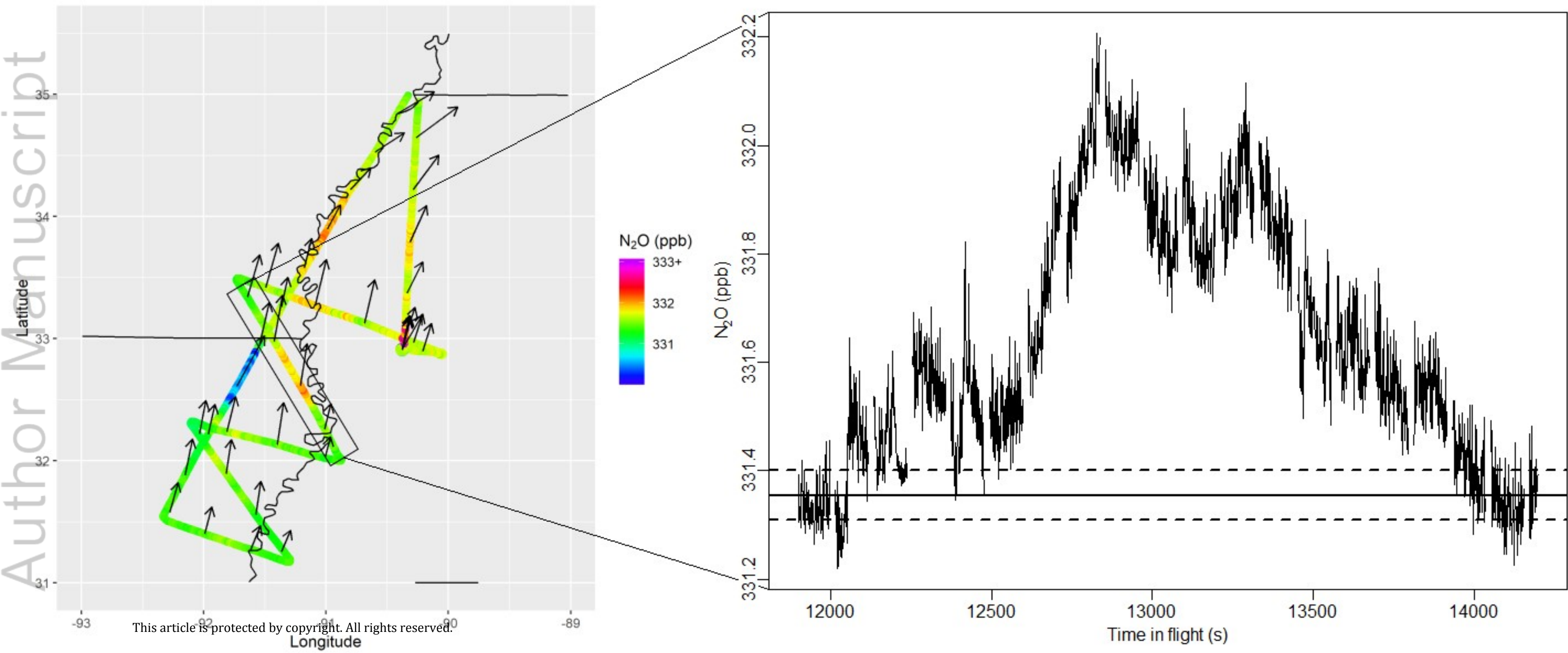
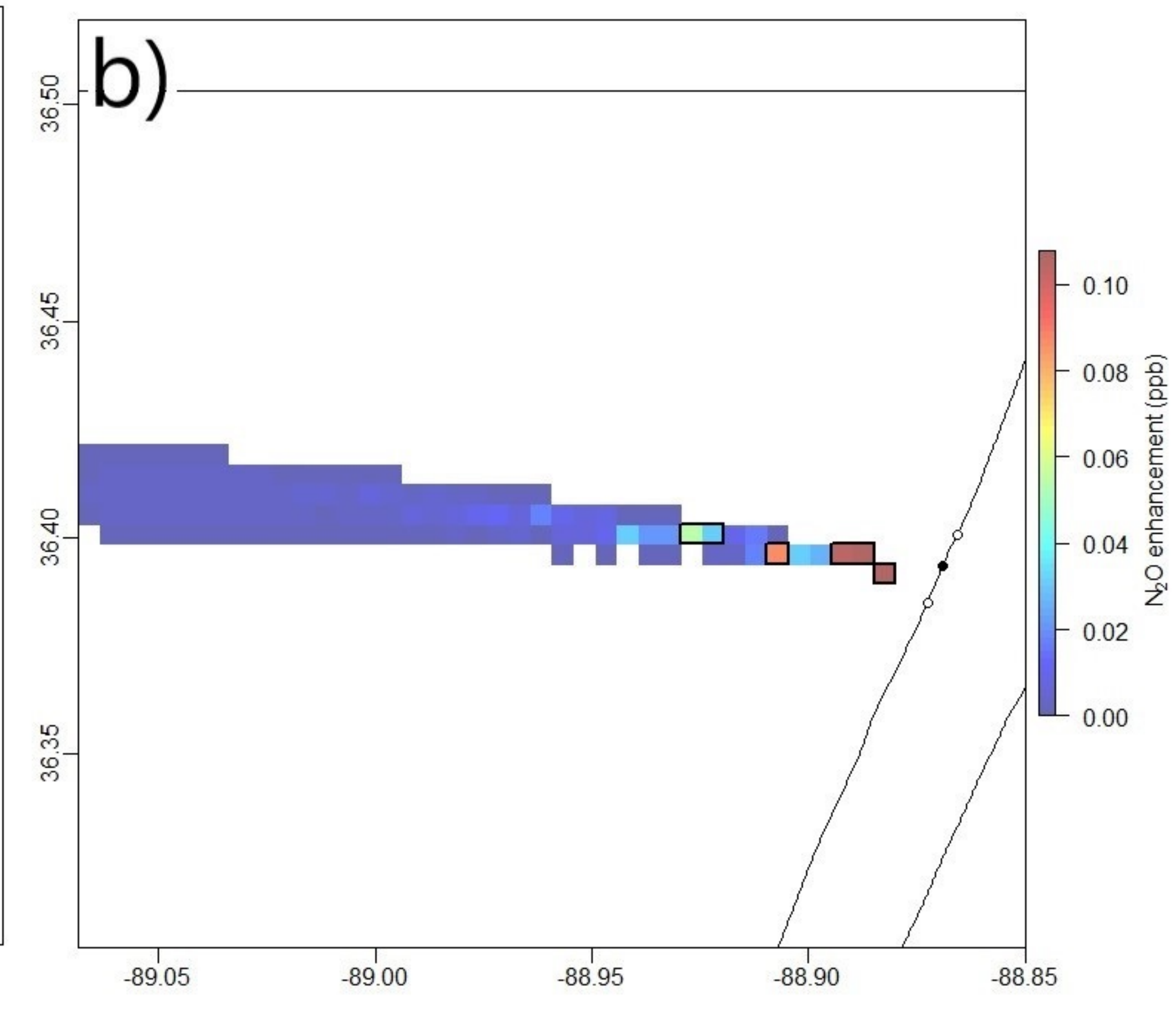
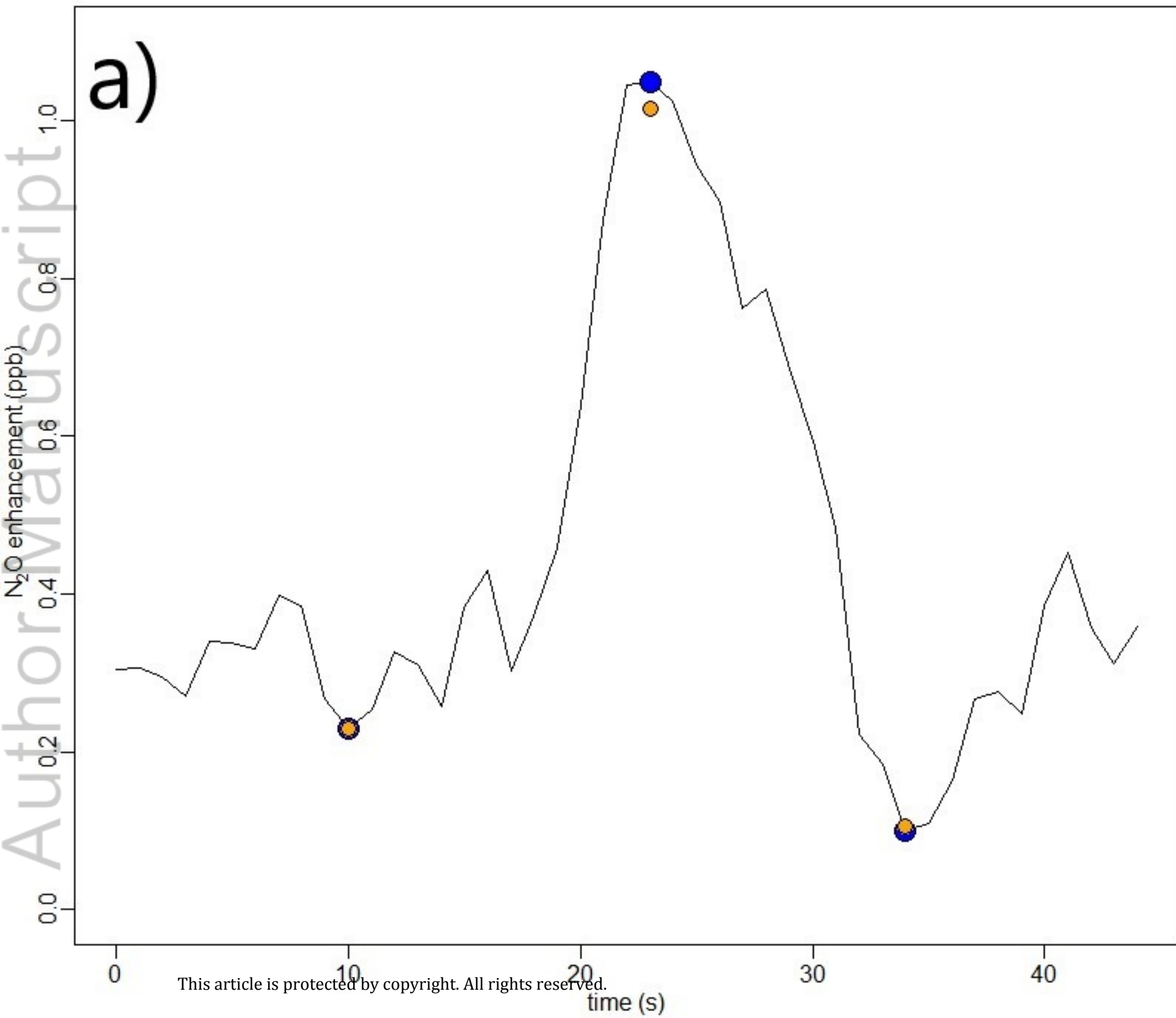
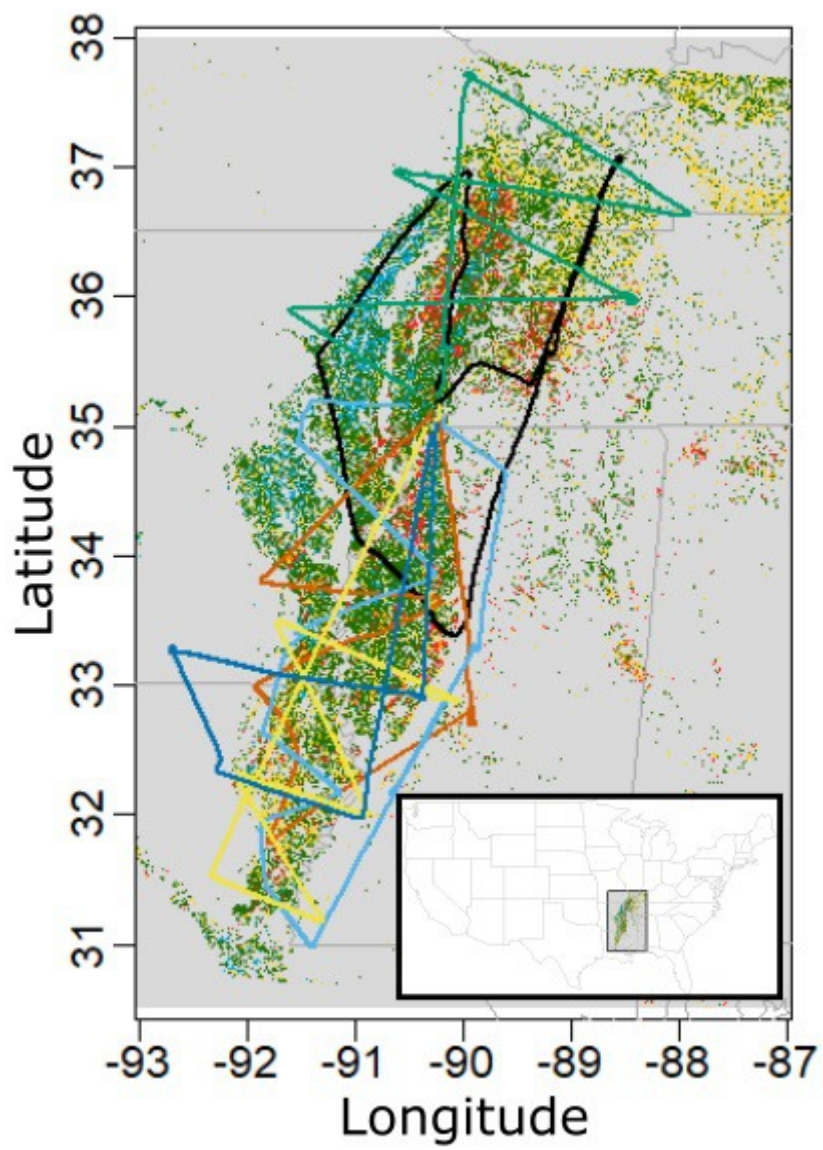


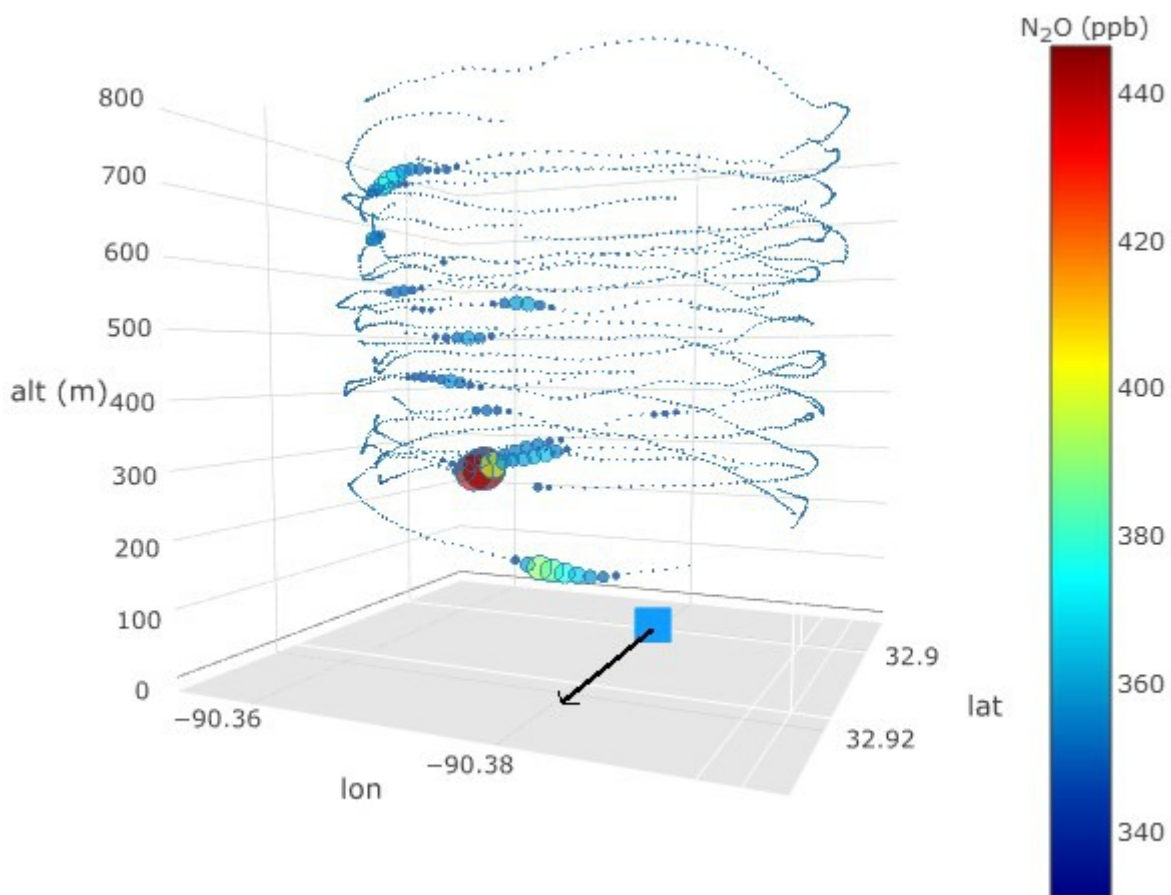
Figure 5.

Author Manuscript

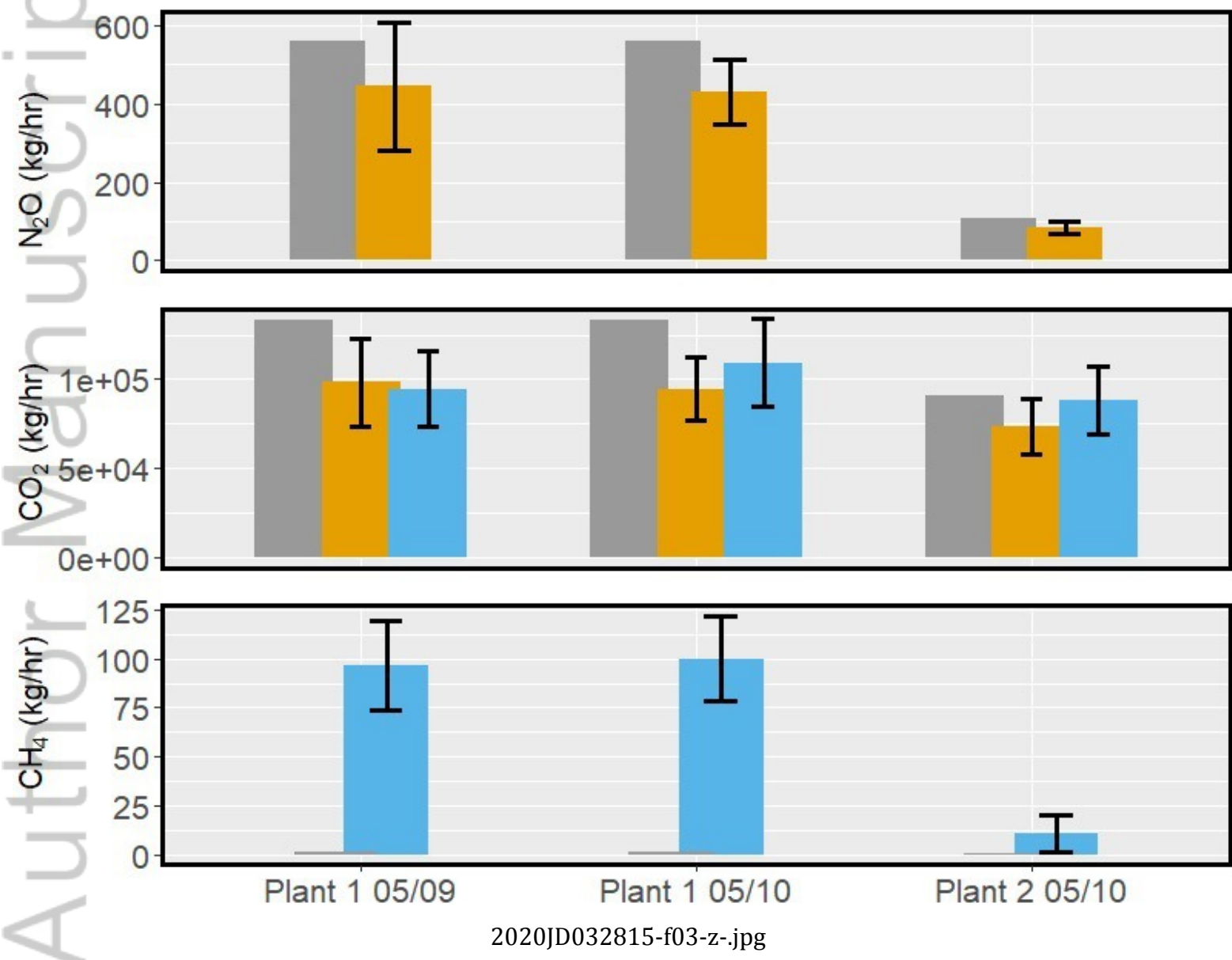




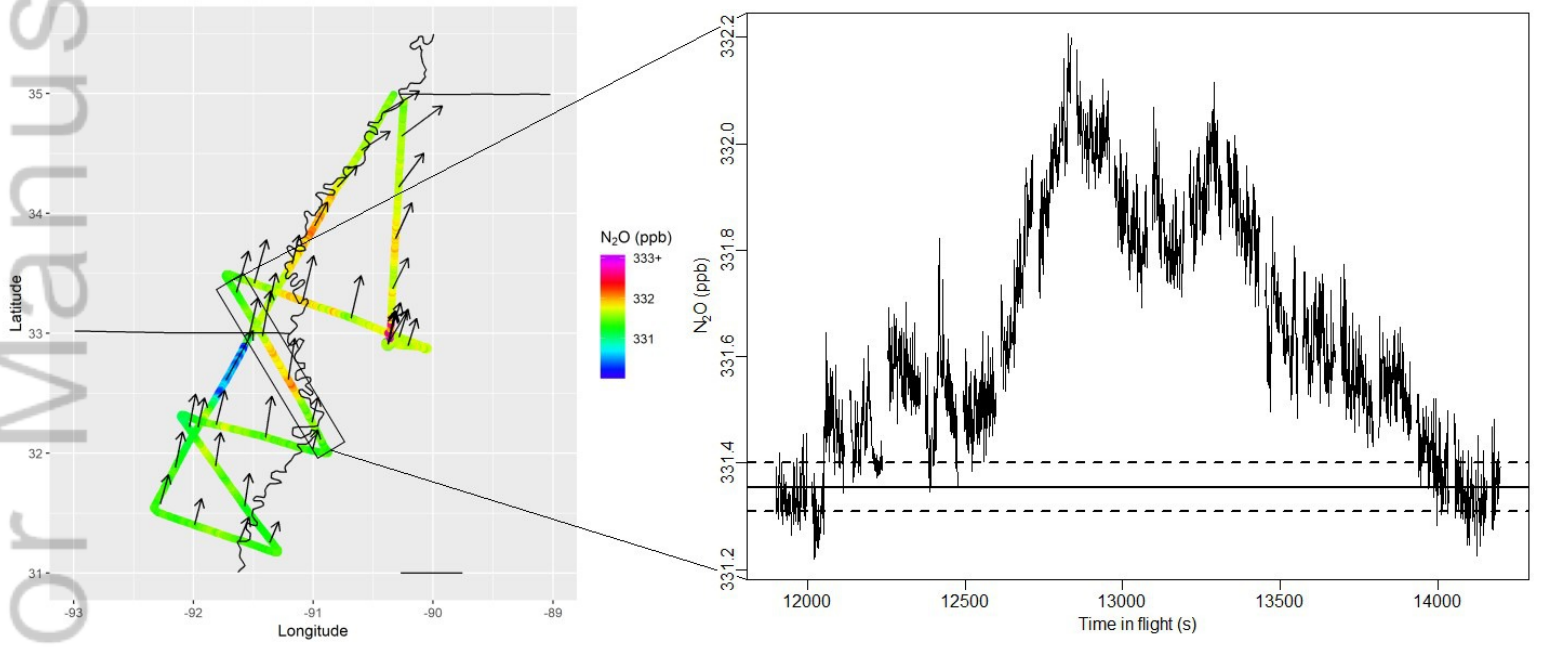
2020JD032815-f01-z-.jpg



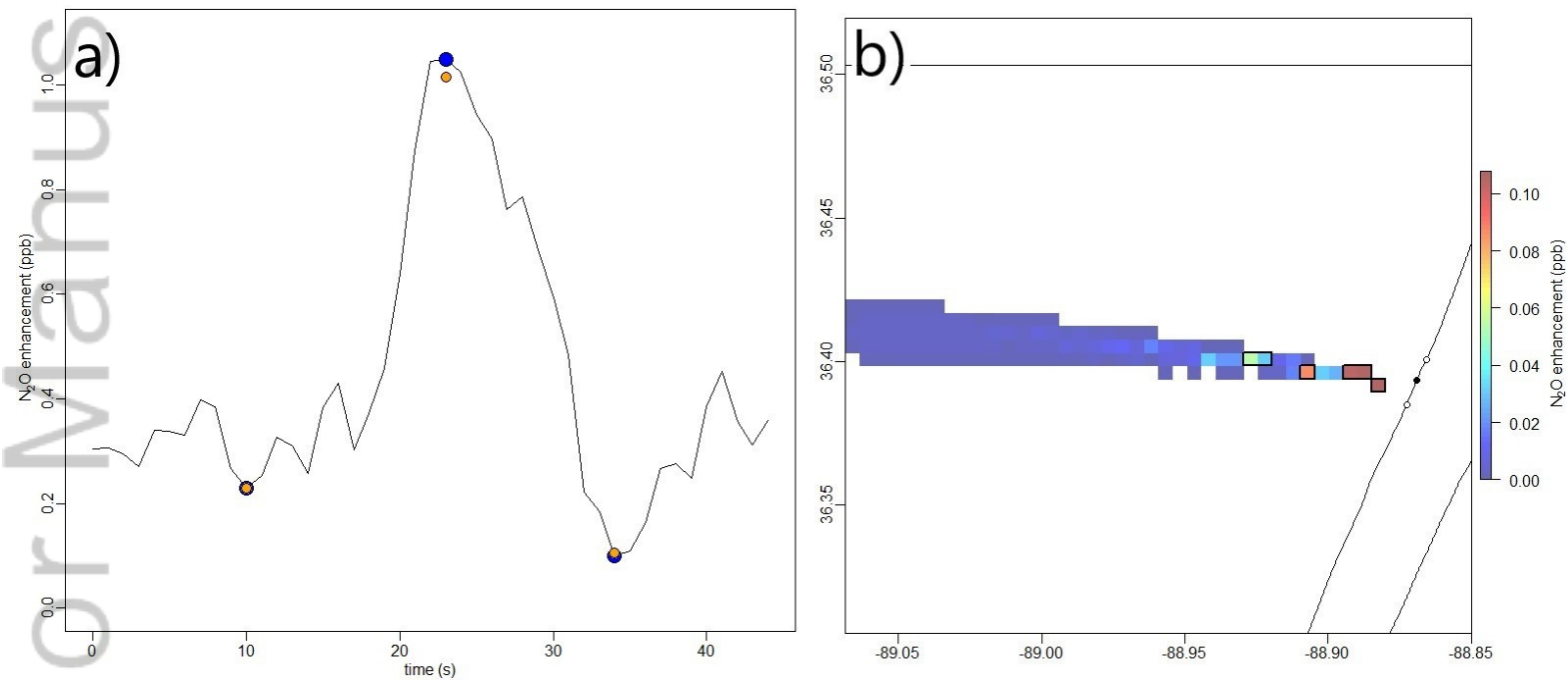
2020JD032815-f02-z-.jpg



2020JD032815-f03-z-.jpg



2020JD032815-f04-z-.jpg



2020JD032815-f05-z-jpg